

Global phase diagrams of binary dipolar fluid mixtures

I. Szalai^{1,*} and S. Dietrich^{2,3,†}

¹*Department of Physics, University of Veszprém, H-8201 Veszprém, POBox 158, Hungary*

²*Max-Planck-Institut für Metallforschung, Heisenbergstr. 3, D-70569 Stuttgart, Germany, and*

³*Institut für Theoretische und Angewandte Physik,
Universität Stuttgart, Pfaffenwaldring 57, D-70569 Stuttgart, Germany*

(Dated: September 28, 2018)

We apply a modified mean-field density functional theory to determine the phase behavior of binary mixtures of Stockmayer fluids whose spherical constituents interact according to Lennard-Jones (LJ) pair potentials with embedded pointlike dipole moments. On the basis of systematic numerical calculations we construct the global phase diagrams of these systems in the three-dimensional thermodynamic space of temperature, pressure, and chemical potential difference of the two components. The vapor-liquid, isotropic liquid – isotropic liquid, isotropic liquid – ferromagnetic liquid, and ferromagnetic liquid – ferromagnetic liquid first-order phase separations are investigated. The loci of the second-order isotropic fluid – ferromagnetic fluid transition are calculated from Landau theory. Liquid-vapor and liquid-liquid critical lines, tricritical lines, triple lines, and lines of critical end points of the binary Stockmayer mixtures are also determined. We discuss how the topology of the phase diagrams change upon varying the strengths of the two dipole moments of the two species as well as their sizes.

PACS numbers: 64.10.+h, 64.75.+g, 68.18.Jk, 64.70.-p

I. INTRODUCTION

There are various classes of fluids whose structural and thermodynamical properties are strongly influenced by the presence of either magnetic or electric dipolar interactions between their constituents: polar molecular liquids, dipolar liquid crystals, ferrofluids, and magneto- or electrorheological fluids. These systems respond to external electric or magnetic fields and some may even exhibit long-ranged spontaneous orientational order in the liquid phases. The strongly anisotropic and long-ranged character of the dipolar forces causes particular difficulties for the theoretical description of these systems. By using simulations, integral equation theories, density functional theories, and phenomenological approaches significant progress has been achieved in understanding one-component dipolar fluids (see, e.g., Refs. [1] and [2] and references therein) albeit several aspects remain still under debate [3].

If isotropic phases of dipolar fluids form interfaces (such as liquid-vapor or fluid-wall interfaces) the broken translational invariance gives rise to interesting local orientational order tied to the interface [4, 5, 6, 7, 8]. Recently such orientational profiles have become experimentally accessible through ellipsometry [9, 10, 11, 12]. In these experiments the orientational order at (critical) liquid-liquid [9, 10] and at (noncritical) fluid-vapor [11, 12] interfaces of several binary mixtures of polar (A) and nonpolar (B) components have been studied. In particular the growing spatial extension of orientational order normal to the interface and proportional to the bulk correlation length upon approaching the continuous demixing transition of A-rich and B-rich phases in the bulk has been analysed. These data have been discussed in terms of universal scaling functions. Various forms of their shape have been proposed [9, 10], including the occurrence of a surface correlation length different from the bulk correlation length [11, 12]. These surprising interpretations lack systematic theoretical analyses, which are particularly important because the ellipsometry data provide only indirect access to orientational profiles so that theoretical guidance is required. It is our goal to provide such systematic theoretical studies for the aforementioned interfacial phenomena near continuous demixing and to extend them to wetting phenomena. As a necessary first step the present work aims at providing an overview of the global phase behavior of polar binary liquid mixtures. This is an indispensable prerequisite for studying the interfacial properties in a second step. Moreover, in view of the numerous interesting features even of bulk properties of dipolar fluids [1, 2, 3], the analysis of dipolar mixtures is also important in its own right.

Already some time ago there was an interesting first step towards the understanding of interfacial properties of dipolar liquid mixtures. In a combined experimental and theoretical study the liquid-vapor surface tensions of two

*Electronic address: szalai@almos.vein.hu

†Electronic address: dietrich@mf.mpg.de

polar binary liquid mixtures have been studied for various temperatures and as function of composition [13]. Using density functional theory (DFT) also relative adsorption as well as concentration and orientational profiles have been calculated [13]. By resorting to an improved DFT it is our intention to expand the above analysis towards focusing on liquid-liquid demixing transitions, the formation of phases with long-ranged orientational order, critical phenomena, and wetting phenomena and thus reaching out to the aforementioned more recent experimental studies.

There is a sizeable body of theoretical research available which is devoted to the study of bulk properties of polar liquid mixtures. This encompasses Monte Carlo simulations [14, 15, 16, 17, 18, 19, 20, 21, 22, 23], molecular dynamics simulations [16, 24, 25, 26, 27, 28, 29], integral equations [30, 31, 32, 33], cluster aggregation models [34, 35, 36, 37, 38], construction of equations of state [39], thermodynamic perturbation theory [40, 41, 42, 43], structure formation in external fields [44], and van der Waals and Ising fluids [45]. There are few theoretical studies concerning the structure formation of dipolar mixtures at interfaces such as DFT and Monte Carlo studies at charged walls [46, 47] and integral equation approaches for dipolar mixtures in random confined geometries [48, 49]. Beyond the aforementioned study in Ref. [13] the structure of dipolar mixtures at interfaces between fluid phases has been investigated by Monte Carlo simulations of the liquid-liquid benzene-water interface [50] and by molecular dynamics simulations [51] and lattice-gas models [52] of the liquid-vapor interface of water-methanol mixtures. In the context of this body of research the present study is focused on obtaining global phase diagrams using an appropriate version of DFT which opens the possibility for interfacial studies later on.

Models for dipolar fluids have to capture three basic features of the pair potentials between the fluid particles: short-ranged repulsion (which in general is anisotropic reflecting molecular shapes), long-ranged attractive dispersion forces (containing an omnipresent isotropic contribution $\sim r^{-6}$ at large distances r between the particles plus higher order anisotropic terms), and the dipolar interaction $\sim r^{-3}$.

As long as one is not aiming for a quantitative description of a specific system but for general phenomena and trends the so-called Stockmayer model has turned out to be rather useful (see Refs. [1] and [2] and references therein). It considers spherical particles interacting with Lennard-Jones (LJ) potentials plus pointlike permanent dipoles at the center. Such binary systems are characterized by three thermodynamic parameters (temperature T and two chemical potentials μ_A and μ_B for the two species A and B), three LJ interaction energy parameters ϵ_{ij} ($i, j = A, B$), three LJ molecular diameter parameters σ_{ij} , and two dipole moments m_A and m_B . After choosing an energy scale for $k_B T = \beta^{-1}$ and the μ_i among the ϵ_{ij} and a length scale for the number densities among the σ_{ij} one is left with a six-dimensional interaction parameter space. By using DFT we analyze the three-dimensional $(T, p, \Delta\mu)$ phase diagrams (where p is the pressure of the system and $\Delta\mu = \mu_B - \mu_A$) as they change along certain paths within suitable subspaces of this interaction parameter space.

This Stockmayer model provides an approximate model for dipolar molecular fluids as well as an effective model for ferrofluids with the solvent degrees of freedom taken into account via *effective* interaction energies ϵ_{ij} . Ferrofluids are often polydisperse [21, 53]. In this respect the study of binary Stockmayer models provides also insight into the effects of polydispersity for ferrofluids in the special case of bimodal distributions of their sizes or of their magnetic moments.

Whereas one-component fluids with simple, radially symmetric pair potentials give rise to only two fluid phases, i.e., liquid and vapor, binary fluids exhibit typically three fluid phases: vapor, A -rich liquid, and B -rich liquid. The latter two emerge via phase segregation from a homogeneous liquid upon lowering the temperature. There is a line of critical points (with high temperatures) limiting a two-dimensional sheet of first-order liquid-vapor phase transitions, a line of critical points (at intermediate temperatures) limiting a two-dimensional sheet of first-order demixing transitions into A -rich and B -rich liquid, and a triple line of phase coexistence between all three fluid phases formed as the intersection of the two aforementioned sheets; at high temperatures the triple line ends at a critical end point where the line of critical demixing points meets the sheet of liquid-vapor coexistence (see, e.g., Ref. [54] and references therein). At low temperatures freezing sets in such that there the triple line ends in a tetra point where the vapor phase, A -rich liquid, B -rich liquid, and the solid phase coexist. (For the topology of this phase diagram see Ref. [55].) In the present study we focus on sufficiently high temperatures so that freezing is not of concern. (For freezing in one-component dipolar fluids see Ref. [2] and references therein. For quasicrystalline order and glasslike structure formation in two-dimensional binary dipolar systems see Refs. [56, 57, 58].) The introduction of dipole moments shifts these phase boundaries and may even give rise to the formation of new liquid phases with spontaneous long-ranged orientational order.

In a recent series of papers [59, 60, 61] Range and Klapp have also extended the modified mean-field density functional theory to study the phase behavior of binary dipolar mixtures. There they have focused on the investigation of the isotropic fluid – ferromagnetic fluid phase separations. Studying dipolar hard sphere mixtures (and briefly mentioning binary Stockmayer fluid mixtures in Ref. [60]) they have found that the isotropic fluid – ferromagnetic fluid phase transitions are shifted towards higher densities as compared with the corresponding one-component dipolar fluids. These general trends are in agreement with our findings for the corresponding phase transitions in binary Stockmayer fluid mixtures. However, there are important differences to the case of dipolar hard sphere systems,

because due to the additional presence of isotropic dispersion forces Stockmayer fluids exhibit also a vapor phase, which is indispensable for studying the interfacial properties mentioned at the beginning of the Introduction. These dispersion forces modify also the other phase transitions. Therefore in the following we explore the wider phase behavior of binary Stockmayer fluid mixtures. In Sec. II we formulate the DFT for Stockmayer fluid mixtures. Our results are presented in Sec. III and summarized and discussed in Sec. IV.

II. DENSITY FUNCTIONAL THEORY FOR STOCKMAYER FLUID MIXTURES

A. Microscopic model

We study binary Stockmayer fluids which consist of spherically symmetric particles interacting via Lennard-Jones (LJ) potentials with parameters σ_{ij} and ϵ_{ij} ($i, j = A, B$):

$$w_{ij}^{LJ}(r_{12}) = 4\epsilon_{ij} \left[\left(\frac{\sigma_{ij}}{r_{12}} \right)^{12} - \left(\frac{\sigma_{ij}}{r_{12}} \right)^6 \right]. \quad (1)$$

In the following for the unlike LJ size parameter we assume $\sigma_{ij} = (\sigma_{ii} + \sigma_{jj})/2$. In addition there is the dipolar interaction due to point dipoles embedded at the centers of spheres of diameter σ_{ii} :

$$w_{ij}^{dip}(\mathbf{r}_{12}, \omega_1, \omega_2) = -\frac{m_i m_j}{r_{12}^3} \left[\frac{[\widehat{\mathbf{m}}_1(\omega_1) \cdot \mathbf{r}_{12}] [\widehat{\mathbf{m}}_2(\omega_2) \cdot \mathbf{r}_{12}]}{r_{12}^2} - [\widehat{\mathbf{m}}_1(\omega_1) \cdot \widehat{\mathbf{m}}_2(\omega_2)] \right] \Theta(r_{12} - \sigma_{ij}) \quad (2)$$

where particle 1 (2) of type i (j) is located at \mathbf{r}_1 (\mathbf{r}_2) and carries a dipole moment of strength m_i (m_j) with an orientation given by the unit vector $\widehat{\mathbf{m}}_1(\omega_1)$ ($\widehat{\mathbf{m}}_2(\omega_2)$) with polar angles $\omega_1 = (\theta_1, \phi_1)$ ($\omega_2 = (\theta_2, \phi_2)$); $\mathbf{r}_{12} = \mathbf{r}_1 - \mathbf{r}_2$ is the difference vector between the centers of the particle i and the particle j with $r_{12} = |\mathbf{r}_{12}|$ and $\Theta(r)$ is the Heaviside step function. Thus the total pair potential is given by

$$w_{ij}(\mathbf{r}_{12}, \omega_1, \omega_2) = w_{ij}^{LJ}(r_{12}) + w_{ij}^{dip}(\mathbf{r}_{12}, \omega_1, \omega_2). \quad (3)$$

In order to apply density functional theory, following Barker and Henderson [62] this interaction potential is decomposed into a short-ranged repulsive reference part

$$w_{ij}^{ref}(r_{12}) = \Theta(\sigma_{ij} - r_{12}) w_{ij}(\mathbf{r}_{12}, \omega_1, \omega_2) = \Theta(\sigma_{ij} - r_{12}) w_{ij}^{LJ}(r_{12}) \quad (4)$$

and into a long-ranged attractive excess part

$$w_{ij}^{exc}(\mathbf{r}_{12}, \omega_1, \omega_2) = \Theta(r_{12} - \sigma_{ij}) w_{ij}(\mathbf{r}_{12}, \omega_1, \omega_2). \quad (5)$$

This decomposition allows one to choose a suitable reference system (a hard sphere system with temperature dependent diameters) for which reliable approximations for the free energy are known. The excess part $w_{ij}^{exc}(\mathbf{r}_{12}, \omega_1, \omega_2)$ is treated perturbatively in a suitable way (see below).

B. Modified mean-field density functional theory

Our analysis is based on the following grand canonical variational functional, which is the binary extension of the one component functional used in Refs. [63] and [64]:

$$\frac{\Omega}{V} = f_{HS}^{ref}(\rho_A, \rho_B, T) + \beta^{-1} \sum_{i=A,B} \rho_i \int d\omega \alpha_i(\omega) \ln[4\pi\alpha_i(\omega)] + \frac{\Omega_{int}}{V} + \sum_{i=A,B} \rho_i \mu_i, \quad (6)$$

where V , T , and μ_i denote the volume of the fluid, its temperature, and the chemical potential of the i th component, respectively, $\beta = 1/(k_B T)$ with the Boltzmann constant k_B , $\rho_i = N_i/V$ is the number density of the species i taken to be spatially constant for the present bulk study. $\alpha_i(\omega)$ is the orientational probability density distribution (i.e., $\rho_i(\omega) = \rho_i \alpha_i(\omega)$ with $\int d\omega \alpha_i(\omega) = 1$ is the number density of particles of type i with orientation ω). The first term in Eq. (6) is the free energy density of the reference system due to Mansoori et al. [65]:

$$f_{HS}^{ref}(\rho_A, \rho_B, T) = \beta^{-1} \sum_{i=A,B} \rho_i [\ln(\Lambda_i^3 \rho_i) - 1] + \beta^{-1} \frac{6}{\pi} \left[\left(\frac{\xi_2^3}{\xi_3} - \xi_0 \right) \ln(1 - \xi_3) + \frac{3\xi_1 \xi_2}{1 - \xi_3} + \frac{\xi_2^3}{\xi_3(1 - \xi_3)^2} \right] \quad (7)$$

where Λ_i denotes the thermal de Broglie wavelength of the particles i and

$$\xi_k = \frac{\pi}{6} \sum_{i=A,B} \rho_i (d_{ii})^k, \quad k = 0, 1, 2, 3 \quad , \quad (8)$$

with temperature dependent hard sphere diameters as given by Barker and Henderson [62]:

$$d_{ii}(T) = \int_0^{\sigma_{ii}} dr_{12} (1 - \exp(-\beta w_{ii}^{ref}(r_{12}))). \quad (9)$$

For $\sigma_{AA} = \sigma_{BB}$ Eq. (7) reduces to the Carnahan-Starling formula. In Eq. (6) the second contribution to the grand canonical functional takes into account the loss of entropy if the orientational distributions of the particles are not isotropic. For the interaction contribution due to the long-ranged part of the pair potential between the spherical particles with embedded point dipoles we adopt

$$\frac{\Omega_{int}}{V} = \frac{1}{2\beta} \sum_{i,j=A,B} \rho_i \rho_j \int d^3 r_1 \int d^3 r_2 \int d\omega_1 \int d\omega_2 \alpha_i(\omega_1) \alpha_j(\omega_2) \exp(-\beta w_{ij}^{ref}(r_{12})) f_{ij}^{exc}(\mathbf{r}_{12}, \omega_1, \omega_2) \quad (10)$$

where

$$f_{ij}^{exc}(\mathbf{r}_{12}, \omega_1, \omega_2) = 1 - \exp(-\beta w_{ij}^{exc}(\mathbf{r}_{12}, \omega_1, \omega_2)) \quad (11)$$

are the Mayer functions with the excess interaction potential. Equation (10) amounts to using the low-density approximation for the pair distribution functions:

$$g_{ij}(r_{12}) = \exp(-\beta w_{ij}^{ref}(r_{12})). \quad (12)$$

For uniaxial molecules the orientational distribution functions $\alpha_i(\omega)$ depend only on the angle θ and thus allow for the following expansion into Legendre polynomials:

$$2\pi \alpha_i(\omega) = \bar{\alpha}_i(\cos \theta) = \sum_{l=0}^{\infty} \alpha_i^{(l)} P_l(\cos \theta) \quad (13)$$

where

$$\alpha_i^{(l)} = \frac{2l+1}{2} \int_{-1}^1 dx \bar{\alpha}_i(x) P_l(x). \quad (14)$$

Following Refs. [63, 64] in order to calculate the spatial integrals in Eq. (10) we consider a finite volume V which has the shape of a prolate rotational ellipsoid with aspect ratio k ($k \geq 1$). The Mayer functions can be expressed in terms of the rotational invariants $\Phi_{l_1 l_2 l}$ (for the definition of these functions see, e.g., Ref. [64]) so that the corresponding integrals yield

$$\frac{\Omega_{int}}{V} = \sum_{i,j=A,B} \rho_i \rho_j \sum_{l=0}^{\infty} u_{ij}^{(l)} \alpha_i^{(l)} \alpha_j^{(l)} \quad (15)$$

where

$$u_{ij}^{(l)} = -\frac{8\pi}{9} \delta_{l,1} I(k) m_i m_j - \beta^{-1} \frac{4\sqrt{\pi}(-1)^l}{(2l+1)^{3/2}} \int_{\sigma_{ij}}^{\infty} dr_{12} r_{12}^2 \int d\omega_1 d\omega_2 f_{ij}^{exc}(r_{12}, \omega_1, \omega_2, \omega_{12}) \Phi_{ll0}^*(\omega_1, \omega_2, \omega_{12}). \quad (16)$$

Further details of this expansion can be found in Ref. [64]. The function $I(k)$ describes the shape dependence of the grand canonical potential, which enters only via the coefficients $u_{ij}^{(1)}$ and is given as

$$I(k) = \frac{k^2 + 2}{3(k^2 - 1)} - \frac{k}{(k^2 - 1)^{3/2}} \ln \left(k + \sqrt{k^2 - 1} \right). \quad (17)$$

Therefore the grand canonical functional reads

$$\frac{\Omega}{V} = f_{ref}^{HS}(\rho_A, \rho_B, T) + k_B T \sum_{i=A,B} \rho_i \int_{-1}^1 dx \bar{\alpha}_i(x) \ln[2\bar{\alpha}_i(x)] + \sum_{i,j=A,B} \rho_i \rho_j \sum_{l=0}^{\infty} u_{ij}^{(l)} \alpha_i^{(l)} \alpha_j^{(l)} - \sum_{i=A,B} \rho_i \mu_i. \quad (18)$$

The equilibrium configuration for given T , μ_A , and μ_B is determined by minimizing the total grand canonical functional with respect to ρ_A , ρ_B , and the functions $\alpha_A(x)$ and $\alpha_B(x)$:

$$\frac{1}{V} \frac{\partial \Omega}{\partial \rho_i} \bigg|_{\rho_j \neq i, \alpha_i(x)} = 0, \quad i = A, B \quad (19)$$

$$\frac{1}{V} \frac{\delta \Omega}{\delta \alpha_i(x)} \bigg|_{\alpha_j \neq i(x), \rho_i} = 0, \quad i = A, B. \quad (20)$$

Equations (18) and (19) lead to

$$\mu_i^{HS}(\rho_A, \rho_B, T) + k_B T \int_{-1}^1 dx \bar{\alpha}_i(x) \ln[2\bar{\alpha}_i(x)] + 2 \sum_{j=A, B} \rho_j \sum_{l=0}^{\infty} u_{ij}^{(l)} \alpha_i^{(l)} \alpha_j^{(l)} - \mu_i = 0, \quad i = A, B. \quad (21)$$

Equation (20) yields

$$\bar{\alpha}_i(x) = C_i \exp \left(-\beta \sum_{l=1}^{\infty} (2l+1) P_l(x) \sum_{j=A, B} \rho_j u_{ij}^{(l)} \alpha_j^{(l)} \right), \quad i = A, B, \quad (22)$$

with

$$\frac{1}{C_i} = \int_{-1}^1 dx \exp \left(-\beta \sum_{l=1}^{\infty} (2l+1) P_l(x) \sum_{j=A, B} \rho_j u_{ij}^{(l)} \alpha_j^{(l)} \right), \quad i = A, B. \quad (23)$$

For the second term in Eq. (18) one finds after some elementary calculations:

$$\beta^{-1} \int_{-1}^1 dx \bar{\alpha}_i(x) \ln[2\bar{\alpha}_i(x)] = k_B T \ln(2C_i) - 2 \sum_{j=A, B} \rho_j \sum_{l=1}^{\infty} u_{ij}^{(l)} \alpha_i^{(l)} \alpha_j^{(l)}, \quad i = A, B. \quad (24)$$

Equations (14) and (22) lead to a system of coupled nonlinear equations for the coefficients $\alpha_A^{(l)}$ and $\alpha_B^{(l)}$:

$$\alpha_i^{(l)} = \frac{2l+1}{2} \frac{\int_{-1}^1 dx P_l(x) \exp \left(-\beta \sum_{l=1}^{\infty} (2l+1) P_l(x) \sum_{j=A, B} \rho_j u_{ij}^{(l)} \alpha_j^{(l)} \right)}{\int_{-1}^1 dx \exp \left(-\beta \sum_{l=1}^{\infty} (2l+1) P_l(x) \sum_{j=A, B} \rho_j u_{ij}^{(l)} \alpha_j^{(l)} \right)}, \quad i = A, B. \quad (25)$$

Equation (21) together with Eqs. (23) and (24) give the following expressions for the chemical potentials of the two components:

$$\mu_i = \mu_i^{HS} + k_B T \ln(2C_i) + \frac{1}{2} \sum_{j=A, B} \rho_j u_{ij}^{(0)}, \quad i = A, B. \quad (26)$$

The chemical potentials μ_A and μ_B can be eliminated from Eq. (18) and therefore Ω can be expressed as

$$\frac{\Omega}{V} = f_{ref}^{HS}(\rho_A, \rho_B, T) - \sum_{i=A, B} \rho_i \mu_i^{HS}(\rho_A, \rho_B, T) - \sum_{i, j=A, B} \rho_i \rho_j \sum_{l=0}^{\infty} u_{ij}^{(l)} \alpha_i^{(l)} \alpha_j^{(l)}. \quad (27)$$

Due to $\Omega = -pV$ the corresponding pressure of an equilibrium phase as a function of the densities and the temperature is

$$p = -f_{ref}^{HS}(\rho_A, \rho_B, T) + \sum_{i=A, B} \rho_i \mu_i^{HS}(\rho_A, \rho_B, T) + \sum_{i, j=A, B} \rho_i \rho_j \sum_{l=0}^{\infty} u_{ij}^{(l)} \alpha_i^{(l)} \alpha_j^{(l)}. \quad (28)$$

These results show that the knowledge of the functions $u_{ij}^{(l)}(T)$ is necessary to obtain the coefficients $\alpha_i^{(l)}$ of the orientational distribution functions (Eq.(25)) and to obtain the different thermodynamic functions (Eqs. (26-28)).

In computing these functions we use the same approximations as in Ref. [64], i.e., we expand the Mayer functions in Eq. (16) for small dipole moments m_i which allows us to perform the angular integrations analytically. As in Ref. [64] we have determined the expansion coefficients up to $O(m^8)$. This gives a satisfactory accuracy for reduced dipole moments $m_i^* = m_i/\sqrt{\epsilon_{AA}\sigma_{AA}^3} \lesssim 2$ [64]. The omission of the higher order terms implies a truncation in the summations at $l = 4$ in all equations which contain such a summation over l . The corresponding coefficients $u_{ij}^{(l)}(T)$ are:

$$u_{ij}^{(0)} = \frac{8\pi}{\beta} \int_{\sigma_{ij}}^{\infty} dr_{12} r_{12}^2 (1 - \exp(-\beta w_{ij}^{LJ}(r_{12})) - \frac{8\pi\beta}{3\sigma_{ij}^3} m_i^2 m_j^2 I_4(\beta\epsilon_{ij}) - \frac{8\pi\beta^3}{25\sigma_{ij}^9} m_i^4 m_j^4 I_{10}(\beta\epsilon_{ij})), \quad (29)$$

$$u_{ij}^{(1)} = -\frac{8\pi}{9} m_i m_j I(k) - \frac{16\pi\beta^2}{225\sigma_{ij}^6} m_i^3 m_j^3 I_7(\beta\epsilon_{ij}), \quad (30)$$

$$u_{ij}^{(2)} = -\frac{8\pi\beta}{375\sigma_{ij}^3} m_i^2 m_j^2 I_4(\beta\epsilon_{ij}) - \frac{32\pi\beta^3}{6125\sigma_{ij}^9} m_i^4 m_j^4 I_{10}(\beta\epsilon_{ij}), \quad (31)$$

$$u_{ij}^{(3)} = \frac{16\pi\beta^2}{25752\sigma_{ij}^6} m_i^3 m_j^3 I_7(\beta\epsilon_{ij}), \quad (32)$$

and

$$u_{ij}^{(4)} = -\frac{8\pi\beta^3}{99225\sigma_{ij}^9} m_i^4 m_j^4 I_{10}(\beta\epsilon_{ij}) \quad (33)$$

with

$$I_n(y) = \int_1^{\infty} dx x^{-n} \exp[4y(x^{-6} - x^{-12})]. \quad (34)$$

C. Phase equilibria and phase diagrams

The phase diagrams at a given temperature T follow from requiring the equality of the chemical potentials of both components and of the pressure for the densities $\rho_i^{(I)}$ and $\rho_i^{(II)}$ characterizing the coexisting phases I and II:

$$\begin{aligned} \mu_A|_{\rho_i^{(I)}, \bar{\alpha}_i^{(I)}(x)} &= \mu_A|_{\rho_i^{(II)}, \bar{\alpha}_i^{(II)}(x)}, \\ \mu_B|_{\rho_i^{(I)}, \bar{\alpha}_i^{(I)}(x)} &= \mu_B|_{\rho_i^{(II)}, \bar{\alpha}_i^{(II)}(x)}, \\ p|_{\rho_i^{(I)}, \bar{\alpha}_i^{(I)}(x)} &= p|_{\rho_i^{(II)}, \bar{\alpha}_i^{(II)}(x)}. \end{aligned} \quad (35)$$

The functions $\bar{\alpha}_i^{(I)}(x)$ and $\bar{\alpha}_i^{(II)}(x)$ ($i = A, B$) denote the corresponding equilibrium orientational distributions obtained from Eqs. (25) and (22). As mentioned in the Introduction we consider four kinds of two-phase equilibria: isotropic liquid – isotropic vapor, isotropic A-rich liquid – isotropic B-rich liquid, isotropic liquid – ferromagnetic liquid, and ferromagnetic A-rich liquid – ferromagnetic B-rich liquid. For binary fluids Gibbs' phase rule allows for three-phase coexistence lines and four-phase (tetra) coexistence points in the thermodynamic space $(T, p, \Delta\mu)$. For isotropic phases the corresponding equations for the chemical potentials and the pressure are simpler because for them $\bar{\alpha}_i(x) = 1/2$ (i.e., $\alpha_i^{(0)} = 1/2$ and $\alpha_i^{(l)} = 0$ if $l \geq 1$).

In order to locate the surface of critical points separating the isotropic and the ferromagnetic liquid phases by second-order phase transitions, similar as in Ref. [64] we expand the orientation dependent ideal gas contributions to the interaction part Ω_{int} of the grand canonical functional for small deviations from isotropy, i.e., for small $\alpha_i^{(l)}$. Using the results for the one component dipolar fluid with $l = 1$ the leading orientation dependent contribution to the grand canonical potential turns out as

$$\frac{\Delta\Omega}{V} = \sum_{i,j=A,B} \left(\rho_i \rho_j u_{ij}^{(1)} + \frac{2\rho_i}{3\beta} \delta_{ij} \right) \alpha_i^{(1)} \alpha_j^{(1)} + \dots \quad (36)$$

where δ_{ij} is the Kronecker delta symbol. Obviously, for given β , ρ_A , and ρ_B the isotropic configuration minimizes the grand canonical functional if the quadratic form defined by Eq. (36) is positive definite. Provided $\rho_A u_{AA}^{(1)} + 2/(3\beta) > 0$, this quadratic form is positive definite if and only if its determinant is positive [66]. For all the cases studied it turns out that this inequality is satisfied. Thus the zero of the determinant defines the surface which separates the isotropic liquid phase from the ferromagnetic liquid phase:

$$\left(\rho_A u_{AA}^{(1)} + \frac{2}{3\beta} \right) \left(\rho_B u_{BB}^{(1)} + \frac{2}{3\beta} \right) - \rho_A \rho_B \left(u_{AB}^{(1)} \right)^2 = 0. \quad (37)$$

In the one-component limit Eq. (37) reduces to the equation for the critical line given in Ref. [64].

III. RESULTS AND DISCUSSION

In the following we shall use reduced quantities: $T^* = k_B T / \epsilon_{AA}$ as reduced temperature, $\rho^* = (\rho_A + \rho_B) \sigma_{AA}^3$ as reduced total density, $x_i = \rho_i / (\rho_A + \rho_B)$ as the concentration of species i , $p^* = p \sigma_{AA}^3 / \epsilon_{AA}$ as reduced pressure, $\mu_i^* = (\mu_i - k_B T \ln(\Lambda_i^3 / \sigma_{AA}^3)) / \epsilon_{AA}$ as the reduced chemical potential of species i , and $m_i^* = m_i / \sqrt{\epsilon_{AA} \sigma_{AA}^3}$ as the reduced dipole moments. For our numerical analysis we consider the following choices for the Lennard-Jones potential parameters: $\epsilon_{BB} / \epsilon_{AA} = 0.95$, $\epsilon_{AB} / \epsilon_{AA} = 0.75$, and $\sigma_{AA} = \sigma_{BB} = \sigma_{AB}$. The case $\sigma_{AA} \neq \sigma_{BB}$ will be discussed in Subsec. III C. The bulk phase diagrams of the binary dipolar fluid mixtures are calculated in the thermodynamic space spanned by temperature T , pressure p , and the difference of the chemical potentials $\Delta\mu = \mu_B - \mu_A$ of the two components. In order to obtain the phase boundaries in this space for fixed T the corresponding phase equilibrium equations (Eq. (35)) have to be solved simultaneously under the constraint

$$\Delta\mu - \mu_B(\rho_A^I, \rho_B^I, T) + \mu_A(\rho_A^I, \rho_B^I, T) = 0. \quad (38)$$

The pressure p follows from Eq. (28).

A. Binary mixtures of particles with equal size and equal dipole moment

As a first step we have determined the phase diagrams of non-polar binary Lennard-Jones fluid mixtures ($m_A^* = m_B^* = 0$) for the aforementioned parameters. Based on our systematic calculations in the thermodynamic space $(T, p, \Delta\mu)$ these phase diagrams take on shapes as shown schematically in Fig. 1(a). S_1 and S_2 are sheets of first-order phase transitions separating the vapor phase from the fluid phase and the A-rich liquid phase from the B-rich liquid phase, respectively. These sheets are bounded by lines L_1 and L_2 , respectively, of second-order phase transitions marking the onset of liquid-vapor separation (L_1) and demixing (L_2) upon lowering the temperature. The intersection of S_1 and S_2 forms the triple line TL of three-phase coexistence ending at the critical end point CEP where L_2 hits S_1 . This type of phase diagrams corresponds to type II in the classification scheme of phase diagrams of binary fluid mixtures given by Scott and van Konynenburg [67, 68]. For the non-polar binary fluid mixture Fig. 2 presents our numerical results for the pressure-temperature (Fig. 2(a)) and the density-temperature (Fig. 2(b)) phase diagrams for $\Delta\mu^* = 0.3$. At low temperatures ($T < T_{tr}$) the A-rich liquid coexists with the vapor. At the triple point temperature $T_{tr}^* = 1.003$ three phases coexist: vapor, B-rich liquid, and A-rich liquid. Above T_{tr} up to the liquid-vapor critical temperature ($T_c^{(lv)*} = 1.153$) there is coexistence between the vapor and the B-rich liquid and between the A-rich liquid and the B-rich liquid. In the temperature range $T_c^{(lv)} < T < T_c^{(ll)}$ with $T_c^{(ll)*} = 1.429$ there is only coexistence between the A-rich liquid and the B-rich liquid.

Figure 1(b) shows the schematic phase diagram of the binary liquid mixture with the same LJ parameters but with $m_A^* = m_B^* = 1$. The occurrence of a ferromagnetic phase gives rise to the appearance of the sheet S_3 which separates the isotropic liquid at high temperatures from the ferromagnetic liquid at low temperatures. The nature of this sheet S_3 differs from that of S_1 and S_2 in that S_3 is the locus of second-order phase transitions. In the thermodynamic space $(T, p, \Delta\mu)$ the surface S_3 is given by the simultaneous solution of Eqs. (37) and (38). (With the knowledge of ρ_A , ρ_B , and T Eq. (28) gives the corresponding pressure p , using the fact that on S_3 $\alpha_i^{(0)} = 1/2$ and $\alpha_i^{(l)} = 0$ for $l \geq 1$.) The intersection of S_3 and S_1 is a line M_1 of critical end points. Along this line the ferromagnetically critical liquid phase coexists with the isotropic vapor phase. The other line M_2 of critical end points is given by the intersection of the sheets S_2 and S_3 . The sheet S_3 divides the triple line into two parts. The upper part describes isotropic vapor – isotropic B-rich liquid – isotropic A-rich liquid three-phase coexistence, while the lower part describes an isotropic vapor – ferromagnetic B-rich liquid – ferromagnetic A-rich liquid coexistence. Both critical lines L_1 and L_2 are in the isotropic part of the thermodynamic space $(T, p, \Delta\mu)$. Figure 3 shows the corresponding results of our

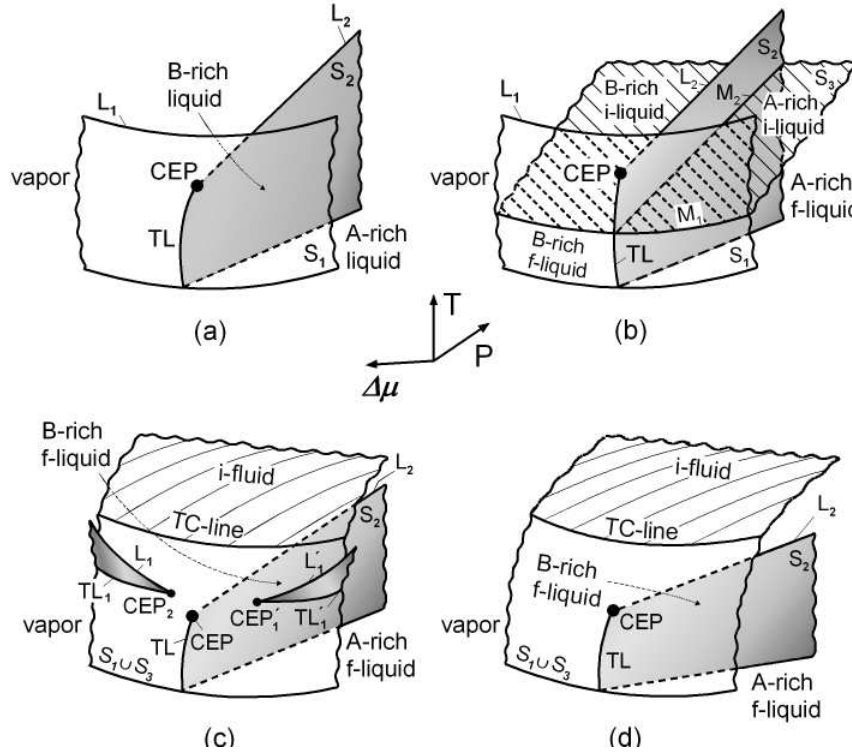


FIG. 1: Schematic bulk phase diagrams of binary Stockmayer fluid mixtures in the thermodynamic space of temperature T , pressure p , and chemical potential difference $\Delta\mu = \mu_B - \mu_A$ of the two components for various equal dipole moments. The phase diagram in (a) represents a non-polar ($m_A^* = m_B^* = 0$) binary fluid mixture which exhibits three phases: vapor, A-rich liquid, and B-rich liquid. They are separated by sheets S_1 and S_2 of first-order phase transitions, delimited by lines L_1 and L_2 , respectively, of second-order phase transitions. S_1 and S_2 intersect along the triple line TL which ends at the critical end point CEP . The phase diagram in (b) represents a dipolar ($m_A^* = m_B^* = 1$) binary fluid mixture for which a third sheet S_3 (hatched) appears, which separates the isotropic liquid from the ferromagnetic liquid. S_3 is a sheet of second-order phase transitions. The intersection of the sheets S_1 and S_3 forms a line M_1 of critical end points. The intersection of the sheets S_2 and S_3 forms another line M_2 of critical end points. Upon increasing the dipole moments ($m_A^* = m_B^* = 1.5$) in (c) the sheet S_3 has been raised above L_1 and has merged with S_1 into the sheet $S_1 \cup S_3$ with a tricritical line (TC-line), which separates the first-order transition (lower part of the sheet) from the second-order transition (hatched upper part). The isotropic liquid-vapor transitions are reduced to two winglike surfaces, which are connected to the sheet $S_1 \cup S_3$ along the triple lines TL_1 and TL'_1 . These triple lines end in critical end points CEP_1 and CEP'_1 . The liquid-vapor critical lines L_1 and L'_1 are the upper edges of the wings. Upon a further increase of the dipole moments ($m_A^* = m_B^* = 2$) one obtains the phase diagram shown in (d) where there are only two sheets: S_2 and $S_1 \cup S_3$. The wings associated with the isotropic liquid – isotropic vapor transitions have disappeared and only the isotropic vapor – ferromagnetic liquid and the ferromagnetic A-rich liquid – ferromagnetic B-rich liquid phase transitions remain.

numerical calculations for a binary Stockmayer fluid mixture with dipole moments $m_A^* = m_B^* = 1$ for $\Delta\mu^* = 0.3$. The intersection of the plane $\Delta\mu^* = 0.3$ with the sheet S_3 yields the critical (dotted) line in Fig. 3(a). Its intersection with the first-order coexistence curve between vapor and ferromagnetic A-rich liquid is the critical end point CEP with $T_{CEP}^* = 1.082$, $p_{CEP}^* = 0.03$, and $\rho_{CEP}^* = 0.74$ at $\Delta\mu^* = 0.3$. Below T_{CEP} the isotropic vapor phase coexists with the ferromagnetic A-rich liquid. The critical line of second-order phase transitions divides the A-rich liquid into an isotropic A-rich liquid phase and into a ferromagnetic A-rich liquid phase. In the temperature range $T_{CEP} < T < T_{tr}$ with $T_{tr}^* = 1.12$ the isotropic vapor coexists with an isotropic A-rich liquid phase. Above the triple point temperature there is also coexistence between the isotropic B-rich liquid and the isotropic A-rich liquid. This first-order phase transition ends in the critical temperature $T_c^{(l)} = 1.404$. The critical temperature of the isotropic vapor – isotropic B-rich liquid coexistence is $T_c^{(lv)} = 1.296$.

Upon increasing the dipole moments the phase diagram shown in Fig. 1(b) changes in two respects. First, the sheet S_3 is raised due to the strengthening of orientational ordering. Second, close to the line M_1 the character of the ferromagnetic - isotropic phase transition on S_3 becomes first-order such that a line of tricritical points (TC) emerges

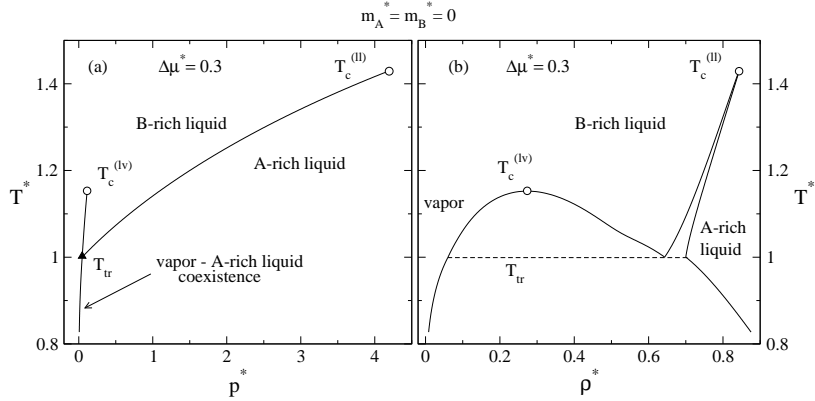


FIG. 2: Phase diagrams of a non-polar ($m_A^* = m_B^* = 0$) binary Lennard-Jones fluid mixture in the pressure-temperature (a) and density-temperature (b) plane for $\Delta\mu^* = 0.3$; $\epsilon_{BB}/\epsilon_{AA} = 0.95$, $\epsilon_{AB}/\epsilon_{AA} = 0.75$, $\sigma_{AA} = \sigma_{BB} = \sigma_{AB}$. T_{tr} , $T_c^{(lv)}$, and $T_c^{(ll)}$ denote the triple, liquid-vapor critical, and liquid-liquid critical temperature, respectively. In (a) all lines are lines of first-order phase transitions. The vapor phase occurs only at very low pressure. In (b) the full curves enclose two-phase regions. The dashed line indicates three-phase coexistence. Below the triple point temperature the vapor coexists with the A-rich liquid. Between T_{tr} and $T_c^{(lv)}$ there are three possible phases: the vapor, the isotropic B-rich liquid, and the A-rich liquid. Between $T_c^{(lv)}$ and $T_c^{(ll)}$ there is only B-rich liquid – A-rich liquid coexistence. At high densities the system freezes. The corresponding solid phases are not shown because they are not accessible by the present theory.

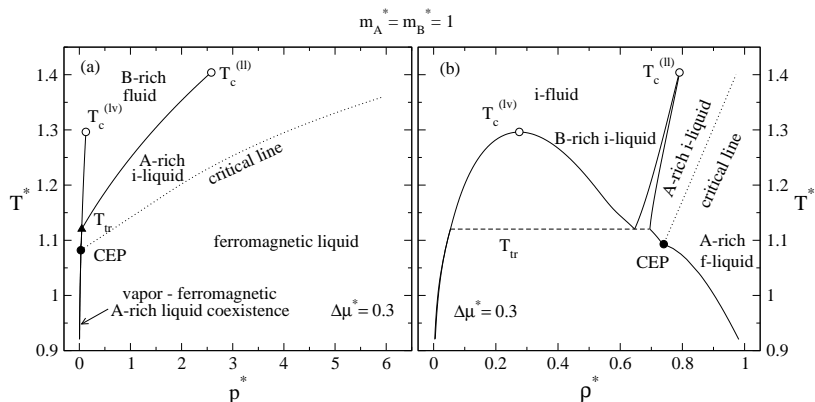


FIG. 3: Phase diagrams of a binary Stockmayer fluid mixture for $m_A^* = m_B^* = 1$ in the pressure-temperature (a) and density-temperature (b) plane for $\Delta\mu^* = 0.3$. The LJ parameters are the same as in Fig. 2. The dotted line denotes a line of second-order phase transitions. It ends at a critical end point (CEP) where the ferromagnetically critical liquid coexists with the non-critical vapor. The critical line divides the A-rich liquid region into an isotropic and ferromagnetic part. For more details see the caption of Fig. 2.

from M_1 and separates the sheet S_3 into a continuous part (back part at high p and hatched) and a first-order part (front part at lower p and unhatched). This implies that M_1 turns into a triple line TL^* . Upon further increase of m_A and m_B this sheet S_3 , divided by the TC -line, raises finally above the line L_2 . Moreover the upper part of S_1 , i.e., above TL^* disintegrates into a left and right part leaving a gap between them. This means that TL^* is split into TL_1 and TL'_1 and L_1 into L_1 and L'_1 in Fig. 1(c). This also generates two critical end points CEP_1 and CEP'_1 which are raised above CEP . Figure 1(c), corresponding to $m_A^* = m_B^* = 1.5$, displays this latter structure with $S_1 \cup S_3$ denoting the sheet which emerged from the lower part of S_1 in Fig. 1(b) and S_3 whereas the winglike structures in Fig. 1(c) are the remnants of the upper part of S_1 in Fig. 1(b). They are connected to the sheet $S_1 \cup S_3$ along the triple lines TL_1 and TL'_1 and bounded by the liquid-vapor critical lines L_1 and L'_1 . The isotropic vapor – isotropic fluid – ferromagnetic liquid triple lines TL_1 and TL'_1 end in critical end points CEP_1 and CEP'_1 . S_2 and $S_1 \cup S_3$

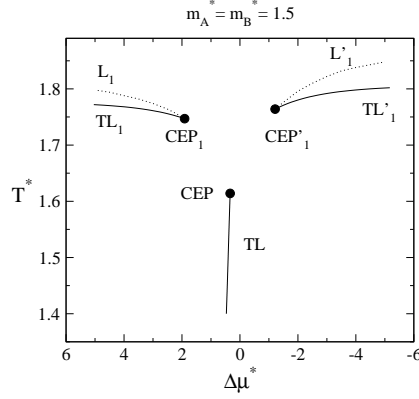


FIG. 4: Projections onto a plane $p = \text{const}$ of the triple lines and of the liquid-vapor critical lines of a binary Stockmayer fluid mixture with $m_A^* = m_B^* = 1.5$; the LJ parameters are the same as in Figs. 2 and 3. In accordance with Fig. 1(c) along TL there is isotropic vapor – A-rich ferromagnetic liquid – B-rich ferromagnetic liquid three phase coexistence. This triple line ends at a critical end point (CEP). Both TL_1 and TL'_1 describe isotropic vapor – isotropic fluid – ferromagnetic fluid three-phase coexistence. These two triple lines end at critical end points CEP_1 and CEP'_1 . The dashed lines L_1 and L'_1 represent the projections of the liquid-vapor critical lines delimiting the upper end of the wings shown in Fig. 1(c). Note that as in Fig. 1 $\Delta\mu$ increases towards the left.

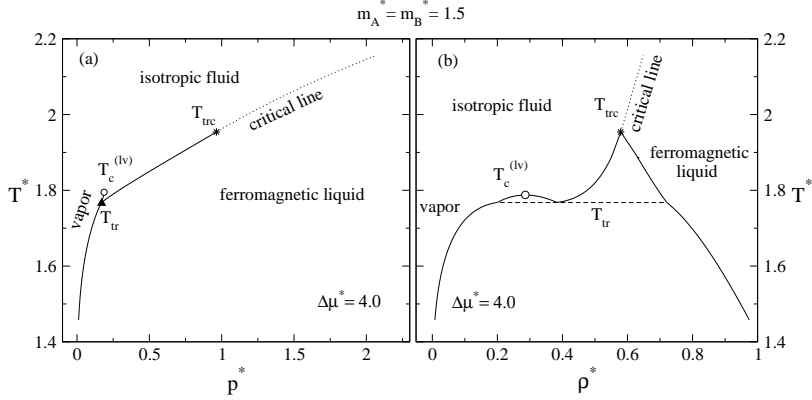


FIG. 5: Phase diagrams of a binary Stockmayer fluid mixture for $m_A^* = m_B^* = 1.5$ (compare Fig. 1(c)) in the pressure-temperature (a) and density-temperature (b) plane for $\Delta\mu^* = 4$; the LJ parameters are the same as in Figs. 2-4. Below the triple point temperature T_{tr} the isotropic vapor coexists with the ferromagnetic liquid. Between T_{tr} and $T_c^{(lv)}$ there are three possible phases: the isotropic vapor, the isotropic liquid, and the ferromagnetic liquid. The first-order phase transition between the isotropic fluid and ferromagnetic liquid turns into a second-order phase transition at the tricritical temperature T_{trc} . Above the tricritical temperature the dotted line represents the corresponding line of critical points. For the value of the chemical potential difference $\Delta\mu^* = 4$ there is no A-rich liquid – B-rich liquid phase separation (i.e., the plane $\Delta\mu^* = 4$ does not intersect the sheet S_2 ; see Figs. 1 and 4). For more details see the caption of Fig. 2.

intersect along the triple line TL which ends at the critical end point CEP .

Figure 4 shows the corresponding results for the projections of the triple lines and of the liquid-vapor critical lines of a binary Stockmayer fluid mixture with dipole moments $m_A^* = m_B^* = 1.5$ onto a plane $p = \text{const}$. The triple line TL describes the isotropic vapor – ferromagnetic A-rich liquid – ferromagnetic B-rich liquid three-phase coexistence with the critical end point temperature $T_{CEP}^* = 1.614$. The triple lines TL_1 and TL'_1 associated with the two winglike surfaces (see Fig. 1(c)) describe the isotropic vapor – isotropic fluid – ferromagnetic A-rich liquid and isotropic vapor – isotropic fluid – ferromagnetic B-rich liquid three-phase coexistences with the critical end point temperatures $T_{CEP'_1}^* = 1.764$ and $T_{CEP_1}^* = 1.747$.

Figure 5 presents our numerical results for a binary Stockmayer fluid mixture with dipole moments $m_A^* = m_B^* = 1.5$

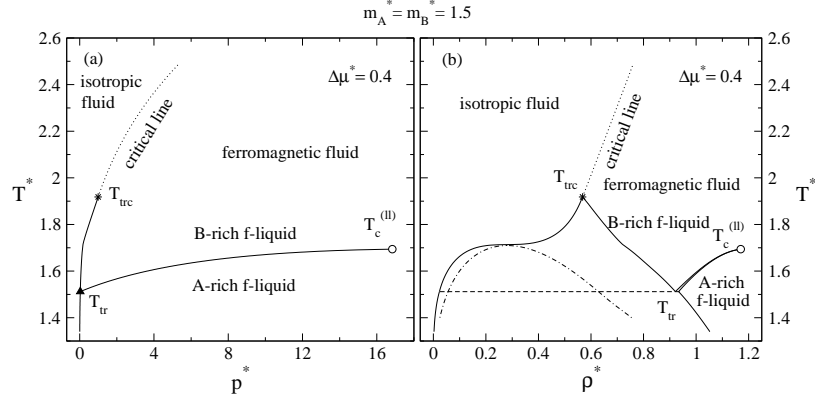


FIG. 6: Phase diagrams of a binary Stockmayer fluid mixture with $m_A^* = m_B^* = 1.5$ (compare Fig. 1(c)) in the pressure-temperature (a) and density-temperature (b) plane for $\Delta\mu^* = 0.4$; the LJ parameters are the same as in Figs. 2-5. For this choice of $\Delta\mu$, below the isotropic vapor – ferromagnetic A-rich liquid – ferromagnetic B-rich liquid triple point temperature T_{tr} the isotropic vapor coexists with the ferromagnetic A-rich liquid. Between T_{tr} and $T_c^{(II)}$ there are three possible phases: the isotropic vapor, the ferromagnetic B-rich liquid, and the ferromagnetic A-rich liquid. In (b) the two-phase region of A-rich and B-rich liquid coexistence ending at $T_c^{(II)}$ is rather narrow. Between $T_c^{(II)}$ and the tricritical temperature T_{trc} the isotropic vapor coexists with the B-rich ferromagnetic liquid. Above the tricritical temperature T_{trc} the transitions between the isotropic and ferromagnetic fluid are continuous and their loci are given by the dotted critical line. The dash-dotted line in (b) indicates the thermodynamically unstable isotropic liquid – vapor coexistence.

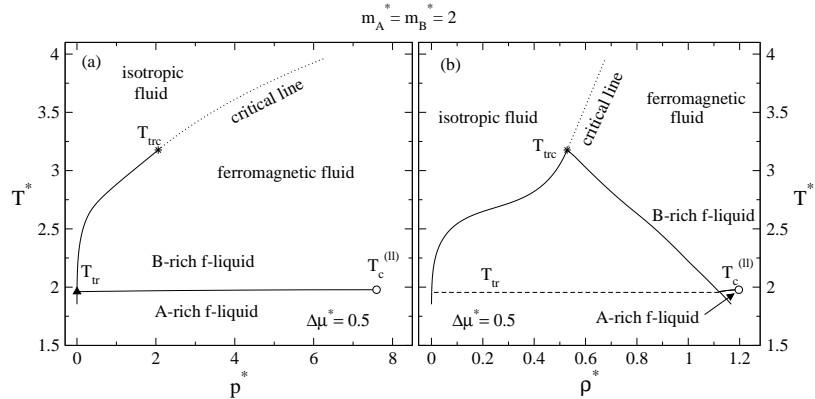


FIG. 7: Phase diagrams of a binary Stockmayer fluid mixture with $m_A^* = m_B^* = 2$ (compare Fig. 1(d)) in the pressure-temperature (a) and density-temperature (b) plane for $\Delta\mu^* = 0.5$; the LJ parameters are the same as in Figs. 2-6. Below the triple temperature T_{tr} the isotropic vapor coexists with a ferromagnetic A-rich liquid. The vapor phase occurs at such small values of p and ρ that it is not visible on the scales shown in (a) and (b). Within the very narrow temperature range $T_{tr} < T < T_c^{(II)}$ there are three possible phases: the isotropic vapor, the ferromagnetic B-rich liquid, and the ferromagnetic A-rich liquid. Above the ferromagnetic B-rich liquid – ferromagnetic A-rich liquid critical temperature $T_c^{(II)}$ there is only coexistence between the isotropic fluid and the B-rich ferromagnetic liquid. Above the tricritical temperature T_{trc} these phase transition are continuous forming the dotted critical line.

for $\Delta\mu^* = 4$. For this choice of $\Delta\mu$ at the triple point T_{tr} the following three phases coexist: vapor, isotropic fluid, and ferromagnetic liquid. At low temperatures $T < T_{tr}$ with $T_{tr}^* = 1.768$ the ferromagnetic liquid coexists with the isotropic vapor. Above the triple point temperature, two isotropic fluids coexist at low and moderate densities, becoming identical above the liquid-vapor critical temperature $T_c^{(lv)*} = 1.788$. (The corresponding critical pressure and density are $p_c^{(lv)*} = 0.185$ and $\rho_c^{(lv)*} = 0.286$, respectively.) At higher densities, the isotropic liquid and magnetic liquid are separated by a first-order phase transition which becomes second order above the tricritical temperature

$T_{trc}^* = 1.954$. (The corresponding tricritical pressure and density are $p_{trc}^* = 0.964$ and $\rho_{trc}^* = 0.579$, respectively.) The critical line of second-order phase transitions divides the liquid range into an isotropic liquid phase and into a ferromagnetic liquid phase. At this value of the chemical potential difference there is no A-rich liquid – B-rich liquid demixing phase separation.

Figure 6 shows our numerical results for a binary Stockmayer fluid mixture with dipole moments $m_A^* = m_B^* = 1.5$ for $\Delta\mu^* = 0.4$. At the triple point temperature T_{tr} the coexisting phases are: vapor, ferromagnetic B-rich liquid, and ferromagnetic A-rich liquid. At low temperatures $T < T_{tr}$ with $T_{tr}^* = 1.512$ the isotropic vapor phase coexists with the ferromagnetic A-rich liquid. Above the triple point temperature, an isotropic vapor coexists with a ferromagnetic B-rich liquid and a ferromagnetic B-rich liquid coexists with a ferromagnetic A-rich liquid. The two ferromagnetic liquid phases become identical beyond the liquid-liquid critical point $T_c^{(ll)}$ with $T_c^{(ll)*} = 1.694$. (The corresponding critical pressure and density are $p_c^{(ll)*} = 16.83$ and $\rho_c^{(ll)*} = 1.17$, respectively, at $\Delta\mu^* = 0.4$.) Above the ferromagnetic A-rich liquid – ferromagnetic B-rich liquid critical temperature $T_c^{(ll)}$ the isotropic liquid and ferromagnetic B-rich liquid are separated by a first-order transition which turns second order above the tricritical temperature $T_{trc}^* = 1.918$. (The corresponding tricritical pressure and density are $p_{trc}^* = 0.994$ and $\rho_{trc}^* = 0.568$, respectively, at $\Delta\mu^* = 0.4$.) At temperatures $T > T_{trc}$ one finds second-order ferromagnetic phase transitions as given by the critical line.

Fig. 1(d) shows that by further increasing the dipole moments ($m_A^* = m_B^* = 2$) the winglike surfaces associated with the isotropic liquid – isotropic vapor transition disappear and only the two sheets S_2 and $S_1 \cup S_3$ remain. Accordingly there is only one triple line TL , which describes the isotropic vapor, ferromagnetic A-rich liquid, and ferromagnetic B-rich liquid three-phase coexistence and which ends at the critical end point CEP where L_2 hits $S_1 \cup S_3$. Since the sheet S_2 bounded by L_2 lies beneath the sheet $S_1 \cup S_3$ all first-order liquid-liquid phase separations involve ferromagnetic phases.

Figure 7 shows our numerical results for a binary Stockmayer fluid mixture with dipole moments $m_A^* = m_B^* = 2$ for $\Delta\mu^* = 0.5$. The topology of Fig. 7 is the same as in Fig. 6, only the numerical values for the triple, critical, and tricritical points are different. Below the triple point temperature $T_{tr}^* = 1.961$ (with $p_{tr}^* = 0.002$ at $\Delta\mu^* = 0.5$) an isotropic vapor coexists with a ferromagnetic A-rich liquid. The ferromagnetic liquid-liquid critical point is given by $T_c^{(ll)*} = 1.98$, $p_c^{(ll)*} = 7.59$, and $\rho_c^{(ll)*} = 1.2$, while the tricritical point is given by $T_{trc}^* = 3.17$, $p_{trc}^* = 2.06$, and $\rho_{trc}^* = 0.528$.

B. Binary liquid mixtures of non-polar and polar particles of equal size

In this subsection we present our results for phase diagrams of non-polar ($m_A^* = 0$) – polar ($m_B^* \neq 0$) binary mixtures. The corresponding schematic phase diagrams are shown in Fig. 8. In order to provide a convenient visual comparison Fig. 8(a) shows again as a reference case the schematic phase diagram of a non-polar binary Lennard-Jones fluid mixture ($m_A^* = m_B^* = 0$) with the parameter set $\epsilon_{BB}/\epsilon_{AA} = 0.95$, $\epsilon_{AB}/\epsilon_{AA} = 0.75$ and $\sigma_{AA} = \sigma_{BB} = \sigma_{AB}$. Figure 8(b) shows the schematic phase diagram of the binary liquid mixture with the same LJ parameters but with $m_A^* = 0$ and $m_B^* = 1$. Similar to Fig. 1(b) the occurrence of a ferromagnetic phase gives rise to the appearance of the sheet S_3 of second-order phase transitions which separates the isotropic liquid phase from the ferromagnetic liquid phase. The ferromagnetic phase appears only in the B-rich liquid phase and at low temperatures while the A-rich liquid phase remains isotropic even at low temperatures. This behavior reflects the polar (B) and non-polar (A) character of molecules. In accordance with this asymmetry the sheet S_3 is tilted, ends at S_2 and thus does not cut through the sheet S_2 . This leads to the line M_2 of critical end points. The intersection of S_3 and S_1 forms another line M_1 of critical end points. The triple line (TL) is given by the intersection of S_1 and S_2 . The line M_1 of critical end points divides the triple line into two parts. The upper part of the triple line describes isotropic vapor – isotropic B-rich liquid – isotropic A-rich liquid three-phase coexistence as in the case of symmetric dipolar mixtures with dipole moments $m_A^* = m_B^* = 1$ (see Fig. 1(b)). The lower part of the triple line describes isotropic vapor – ferromagnetic B-rich liquid – isotropic A-rich liquid coexistence.

Figure 9 shows our numerical findings for a binary Stockmayer fluid mixture with dipole moments $m_A^* = 0$ and $m_B^* = 1$ for $\Delta\mu^* = -0.27$. Figure 9(a) demonstrates that for this value of the chemical potential difference the plane $\Delta\mu^* = -0.27$ cuts through the upper part of the triple line TL in Fig. 8(b) so that the corresponding triple point T_{tr} describes an isotropic vapor – A-rich isotropic liquid – B-rich isotropic liquid coexistence with $T_{tr}^* = 1.16$ and $p_{tr}^* = 0.101$. The intersection of this plane with the sheet S_3 yields the dotted critical line. The intersection of the plane $\Delta\mu^* = -0.27$ with the line M_1 in Fig. 8(b) gives the critical end point CEP where an isotropic vapor coexists with a ferromagnetically critical B-rich liquid. The thermodynamic parameters of this critical end point CEP are given by $T_{CEP}^* = 1.07$, $p_{CEP}^* = 0.043$, and $\rho_{CEP}^* = 0.74$, respectively, for $\Delta\mu^* = -0.27$. Below the temperature T_{CEP} the isotropic vapor phase coexists with the ferromagnetic B-rich liquid phase. Between the temperatures T_{CEP} and T_{tr} two phases coexist: the isotropic vapor and the B-rich isotropic liquid. Above T_{tr} up to the liquid-vapor

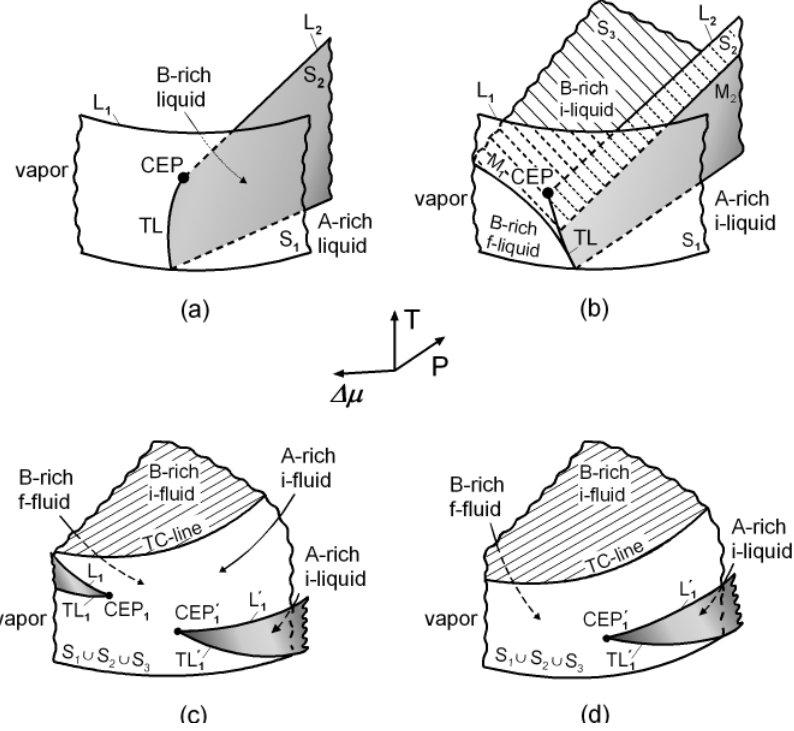


FIG. 8: Schematic bulk phase diagrams of binary Stockmayer fluid mixtures in the thermodynamic space of temperature T , pressure p , and chemical potential difference $\Delta\mu = \mu_B - \mu_A$ of the non-polar ($m_A^* = 0$) and polar ($m_B^* \neq 0$) components. For reference purposes the phase diagram in (a) represents the same non-polar ($m_A^* = m_B^* = 0$) binary fluid mixture as in Fig.1(a). The phase diagram in (b) represents a non-polar – dipolar ($m_A^* = 0, m_B^* = 1$) binary fluid mixture for which in comparison with (a) a third sheet S_3 (hatched) appears, which separates the B-rich isotropic liquid from the B-rich ferromagnetic liquid. S_3 is a sheet of second-order phase transitions. M_1 and M_2 represent lines of critical end points at the intersection of S_3 with S_1 and S_2 , respectively. In (a)-(d) the A-rich liquid is always isotropic. Upon increasing the dipole moment of the component B ($m_A^* = 0, m_B^* = 1.5$) in (c) the tilted sheet S_3 has moved above L_1 and L_2 and has merged with S_1 and S_2 into the sheet $S_1 \cup S_2 \cup S_3$ with a tricritical line (TC-line), which separates first-order transitions (lower part of the sheet) from second-order transitions (hatched upper part). The loci of isotropic liquid – vapor transitions are reduced to two winglike surfaces, which are connected to the surface $S_1 \cup S_2 \cup S_3$ along the triple lines TL_1 and TL'_1 . These triple lines end in critical end points CEP_1 and CEP'_1 . The liquid-vapor critical lines L_1 and L'_1 are the upper edges of the wings. Upon a further increase of the dipole moment of component B ($m_A^* = 0, m_B^* = 2$) one obtains the phase diagram shown in (d) where there is only one sheet $S_1 \cup S_2 \cup S_3$ and one wing attached to it. The surface $S_1 \cup S_2 \cup S_3$ denotes the isotropic vapor – ferromagnetic liquid transition, while the wing is associated with the A-rich isotropic liquid – isotropic vapor transition.

critical temperature ($T_c^{(lv)*} = 1.19$) coexistence is possible between the vapor and the A-rich isotropic liquid phase and between the A-rich isotropic liquid and the B-rich isotropic liquid. In the temperature range $T_c^{(lv)*} < T < T_c^{(ll)}$ with $T_c^{(ll)*} = 1.23$ coexistence is possible only between the isotropic A-rich and B-rich liquid phases. (The corresponding critical densities are $\rho_c^{(lv)*} = 0.31$ and $\rho_c^{(ll)*} = 0.55$, respectively.)

Figure 10 shows our numerical results for a binary Stockmayer fluid mixture with dipole moments $m_A^* = 0$ and $m_B^* = 1$ for $\Delta\mu^* = -0.54$. Figure 10(a) displays that for this value of the chemical potential difference the plane $\Delta\mu^* = -0.54$ cuts through the lower part of the triple line TL in Fig. 8(b) so that the corresponding triple point T_{tr} describes an isotropic vapor – A-rich isotropic liquid – B-rich ferromagnetic liquid coexistence with $T_{tr}^* = 1.05$ and $p_{tr}^* = 0.045$. Below the triple temperature T_{tr} the vapor phase coexists with the B-rich ferromagnetic liquid phase. Above T_{tr} up to the liquid-vapor critical temperature ($T_c^{(lv)*} = 1.21$) coexistence is possible between the vapor and the A-rich isotropic liquid phase and between the A-rich isotropic liquid and the B-rich ferromagnetic liquid. The critical pressure and density of liquid-vapor coexistence are $p_c^{(lv)*} = 0.122$ and $\rho_c^{(lv)*} = 0.285$, respectively. The A-rich isotropic liquid – B-rich ferromagnetic liquid phase coexistence extends to higher temperatures. The corresponding liquid-liquid critical point is not attainable at physically relevant fluid densities. (At high densities the system freezes, but the corresponding solid phases are not captured within the framework of the present theory.)

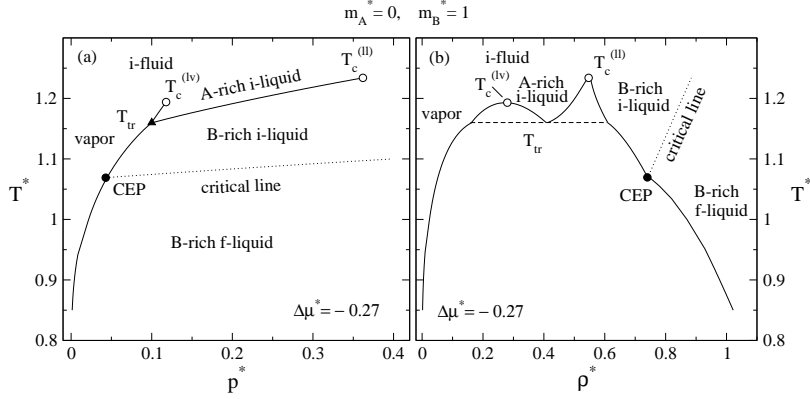


FIG. 9: Phase diagrams of a non-polar – polar ($m_A^* = 0$, $m_B^* = 1$) binary Stockmayer fluid mixture (compare Fig. 8(b)) in the pressure-temperature (a) and density-temperature (b) plane for $\Delta\mu^* = -0.27$. The LJ parameters are the same as in Fig. 2. Below the critical end point (*CEP*) temperature T_{CEP} the isotropic vapor coexists with the B-rich ferromagnetic liquid. Between T_{CEP} and T_{tr} the isotropic vapor coexists with the B-rich isotropic liquid. Between T_{tr} and $T_c^{(iv)}$ there are three possible phases: the vapor, the A-rich isotropic liquid, and the B-rich isotropic liquid. Between $T_c^{(iv)}$ and $T_c^{(II)}$ only A-rich isotropic liquid – B-rich isotropic liquid coexistence is possible. The dotted line denotes a line of second-order ferromagnetic phase transitions. It ends at a critical end point *CEP*.

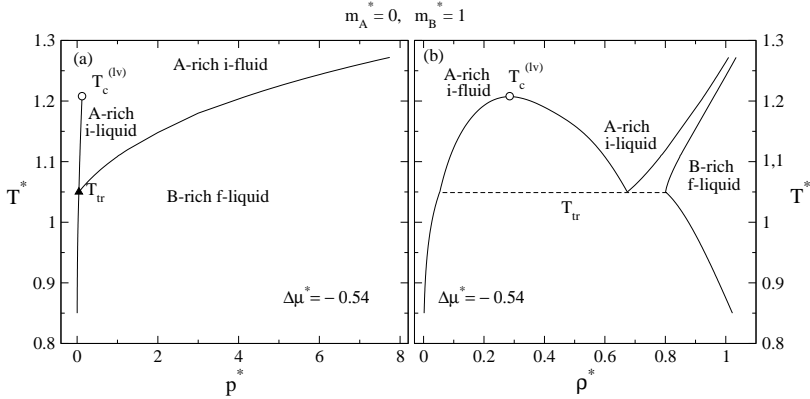


FIG. 10: Phase diagrams of a binary Stockmayer fluid mixture for $m_A^* = 0$ and $m_B^* = 1$ (compare Fig. 8(b)) in the pressure-temperature (a) and density-temperature (b) plane for $\Delta\mu^* = -0.54$; the LJ parameters are the same as in Fig. 2. Below the triple point temperature T_{tr} the isotropic vapor coexists with the B-rich ferromagnetic liquid. Between T_{tr} and $T_c^{(iv)}$ there are three possible phases: the vapor, the A-rich isotropic liquid, and the B-rich ferromagnetic liquid. The A-rich isotropic liquid – B-rich ferromagnetic liquid coexistence does not end in a critical point within the range of fluid densities.

Upon increasing the dipole moment of component *B* the phase diagram shown in Fig. 8(b) changes considerably. First, the sheet S_3 moves up due to the strengthening of the dipolar interaction. Like in the case of symmetrical dipolar mixtures ($m_A^* = m_B^* = 1.5$, see Fig. 1(c)) close to the line M_1 the ferromagnetic-isotropic phase transition on the sheet S_3 becomes first order. This means that a line TC of tricritical points emerges from M_1 and separates the sheet S_3 into a continuous part and a first-order part. In turn this implies that M_1 turns into a triple line TL^* . In the next step due to the rise of the sheet S_3 (divided by the TC -line) the line M_2 rises, too, and merges with the line L_2 so that S_3 and S_2 form a single sheet $S_2 \cup S_3$. Upon a further increase of m_B the upper part of S_1 disintegrates into a left and a right part leaving a gap between them, where S_1 merges with $S_2 \cup S_3$ forming the surface $S_1 \cup S_2 \cup S_3$. The remnants of the upper part of the sheet S_1 appear as asymmetrically winglike structures, where the triple lines TL_1 and TL'_1 stem from the triple line TL^* which has split while the split line L_1 generates the liquid-vapor critical lines L_1 and L'_1 (see Fig. 8(c)). The intersections of the corresponding triple and critical lines give two critical end points

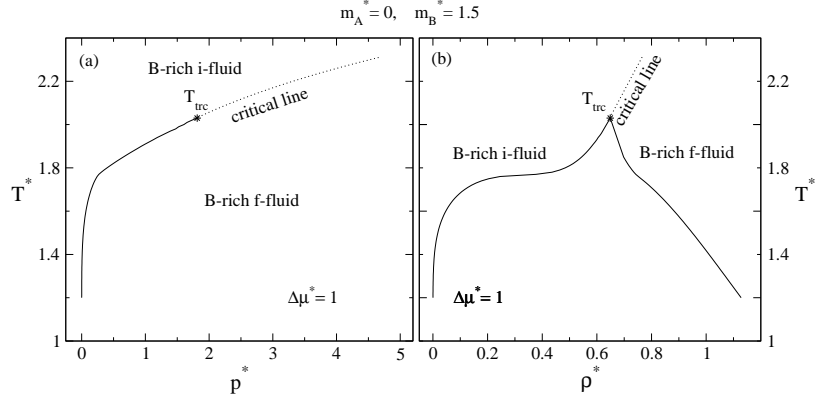


FIG. 11: Phase diagrams of a binary Stockmayer fluid mixture for $m_A^* = 0$ and $m_B^* = 1.5$ (compare Fig. 8(c)) in the pressure-temperature (a) and density-temperature (b) plane for $\Delta\mu^* = 1$; the LJ parameters are the same as in Fig. 2. Below the tricritical temperature T_{trc} the B-rich isotropic fluid coexists with the B-rich ferromagnetic fluid. This first-order phase transition turns into a second-order phase transition at the tricritical temperature T_{trc} . Above T_{trc} the dotted line represents the line of second-order phase transitions.

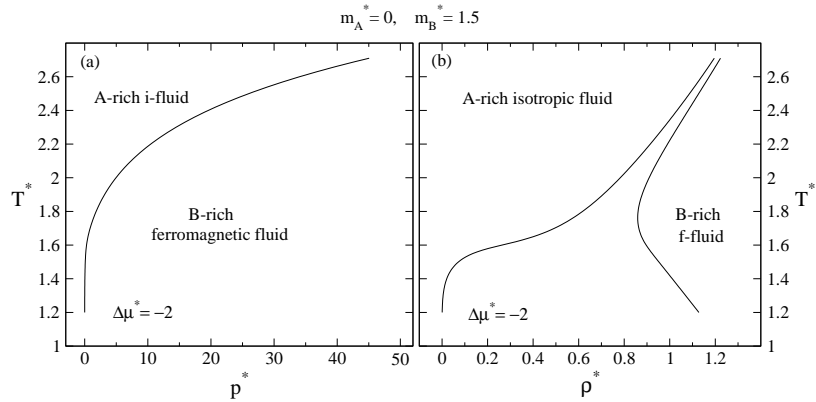


FIG. 12: Phase diagrams of a binary Stockmayer fluid mixture for $m_A^* = 0$ and $m_B^* = 1.5$ (compare Fig. 8(c)) in the pressure-temperature (a) and density-temperature (b) plane for $\Delta\mu^* = -2$; the LJ parameters are the same as in Fig. 2. At this value of the chemical potential difference only the A-rich isotropic liquid can coexist along a line of first-order phase transitions with the B-rich ferromagnetic liquid. The liquid-liquid coexistence does not end in a critical point within the range of physically relevant fluid densities.

CEP_1 and CEP'_1 . Figure 8(c) corresponds to $m_A^* = 0$ and $m_B^* = 1.5$ and displays this final structure with $S_1 \cup S_2 \cup S_3$ denoting the surface which has emerged from the sheets S_1 , S_2 , and S_3 (shown in Fig. 8(b)) upon the increase of the dipole moment m_B .

Figure 11 shows our numerical results for a binary Stockmayer fluid mixture with dipole moments $m_A^* = 0$ and $m_B^* = 1.5$ for $\Delta\mu^* = 1$. For this value of $\Delta\mu^*$ the figure displays a vertical intersection of the phase diagram shown in Fig. 8(c) between the two critical end points CEP_1 and CEP'_1 and close to CEP_1 . At low temperatures the B-rich isotropic fluid and the B-rich ferromagnetic fluid are separated by a first-order phase transition which becomes second order above the tricritical temperature $T_{trc}^* = 2.03$. (The tricritical pressure and density are $p_{trc}^* = 1.82$ and $\rho_{trc}^* = 0.65$, respectively.) The dotted critical line corresponds to a cut through the second-order part of the surface $S_1 \cup S_2 \cup S_3$.

Figure 12 shows our numerical findings for a binary Stockmayer fluid mixture with dipole moments $m_A^* = 0$ and $m_B^* = 1.5$ for $\Delta\mu^* = -2$. This figure displays a vertical cut through the phase diagram in Fig. 8(c) between CEP_1 and CEP'_1 but close to the critical end point CEP'_1 . For this value of the chemical potential difference the A-rich isotropic fluid can coexist with the B-rich ferromagnetic fluid. Note that the B-rich isotropic fluid and the A-rich isotropic

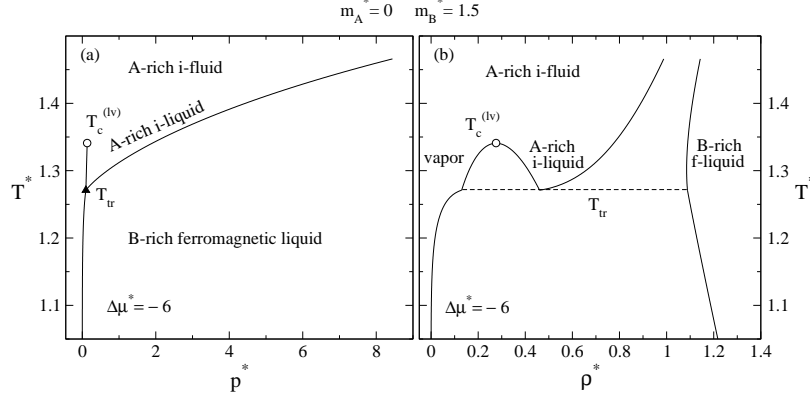


FIG. 13: Phase diagrams of a binary Stockmayer fluid mixture for $m_A^* = 0$ and $m_B^* = 1.5$ (compare Fig. 8(c)) in the pressure-temperature (a) and density-temperature (b) plane for $\Delta\mu^* = -6$; the LJ parameters are the same as in Fig. 2. Below the triple point temperature T_{tr} the isotropic vapor coexists with the B-rich ferromagnetic liquid. Between T_{tr} and $T_c^{(lv)}$ there are three possible phases: the vapor, the A-rich isotropic liquid, and the B-rich ferromagnetic liquid. The A-rich isotropic liquid – B-rich ferromagnetic liquid coexistence does not end in a critical point within the range of physically relevant fluid densities.

fluid are not separated by a demixing transition; in Fig. 8(c) both are in front of $S_1 \cup S_2 \cup S_3$. The liquid-liquid critical point lies outside the physically relevant fluid densities.

Figure 13 shows our numerical results for a binary Stockmayer fluid mixture with dipole moments $m_A^* = 0$ and $m_B^* = 1.5$ for $\Delta\mu^* = -6$. In this case the plane $\Delta\mu^* = -6$ cuts through the wing on the right side of the surface $S_1 \cup S_2 \cup S_3$ in Fig. 8(c). For this choice of $\Delta\mu$ at the triple point T_{tr} the following three phases coexist: vapor, A-rich isotropic liquid, and B-rich ferromagnetic liquid. At low temperatures $T < T_{tr}$ with $T_{tr}^* = 1.27$ ($p_{tr}^* = 0.1$) the B-rich ferromagnetic liquid coexists with the isotropic vapor. Above the triple point temperature at low densities the vapor coexists with the A-rich isotropic liquid, whereas at high densities the A-rich isotropic liquid coexists with the B-rich ferromagnetic liquid. The vapor and the A-rich isotropic liquid merge at the liquid-vapor critical point $T_c^{(lv)*} = 1.34$, $p_c^* = 0.13$, and $\rho_c^* = 0.28$. The A-rich isotropic liquid – B-rich ferromagnetic liquid critical point occurs outside the physically relevant fluid densities.

Figure 8(d) shows that by further increasing the dipole moment of the component B ($m_A^* = 0, m_B^* = 2$) the winglike structure on the left hand side in Fig. 8(c), which is associated with the B-rich isotropic liquid – vapor transitions, disappears so that there remain only the two sheets $S_1 \cup S_2 \cup S_3$ and the wing on the right hand side associated with the A-rich isotropic liquid – vapor transitions. Accordingly there is only one triple line TL'_1 , which describes the isotropic vapor – A-rich isotropic liquid – B-rich ferromagnetic liquid three-phase coexistence. It ends at the critical end point CEP'_1 where L'_1 hits the surface $S_1 \cup S_2 \cup S_3$. Since the topology of the phase diagram in Fig. 8(d) is the same as that of Fig. 8(c) (only the left winglike surface in Fig. 8(c) is missing), the topologies of different cuts at given chemical potentials are in agreement with the topologies of the phase diagrams in Figs. 11-13. Therefore we refrain from presenting our detailed numerical results for Stockmayer mixtures with dipole moments $m_A^* = 0$ and $m_B^* = 2$.

C. Binary liquid mixtures of polar particles of different size

In this subsection we present phase diagrams of binary Stockmayer liquid mixtures of polar particles ($m_A^* \neq m_B^*$) of different size. Since in the Stockmayer interaction potential the size parameters appear in the LJ contribution to the potential, we first study the effect of varying the ratio σ_{BB}/σ_{AA} on the phase diagrams of binary LJ fluid mixtures ($m_A^* = m_B^* = 0$) while keeping the energy parameters of the LJ potential fixed.

Figure 14 shows the projections of the triple lines of binary LJ fluid mixtures with different particle size ratios onto a plane $p = \text{const}$. These triple lines describe the vapor – A-rich isotropic liquid – B-rich isotropic liquid three-phase coexistence. The curves show that the sheet S_2 , which separates the A-rich and B-rich liquid phases (see Fig. 1(a)) is increasingly tilted upon increasing the size ratio σ_{BB}/σ_{AA} . The critical end point temperature increases and the chemical potential difference $\Delta\mu_{CEP}^*$ at the end point turns more negative, i.e., it is shifted towards the region of fluid rich in the small particles. This means that for large size ratios three phase coexistence occurs for a wider range

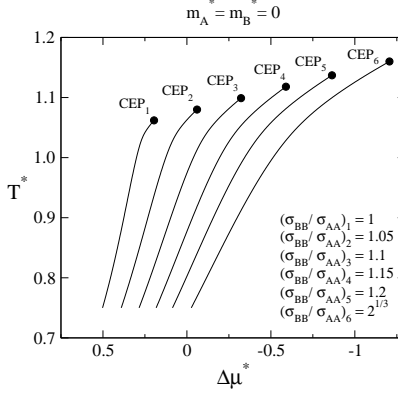


FIG. 14: Projections of the vapor - A-rich isotropic liquid - B-rich isotropic liquid triple line TL (see Fig. 1) of binary Lennard-Jones fluid mixtures ($m_A^* = m_B^* = 0$) onto a plane $p = \text{const}$ for $\epsilon_{BB}/\epsilon_{AA} = 0.95$, $\epsilon_{AB}/\epsilon_{AA} = 0.75$, and various size ratios σ_{BB}/σ_{AA} . The triple lines end at different critical end points (CEPs, see Fig. 1). Note that as in Figs. 1 and 4 $\Delta\mu$ increases towards the left.

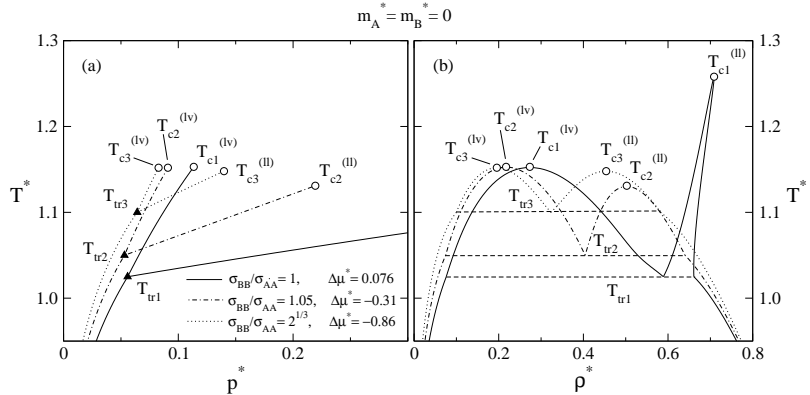


FIG. 15: Phase diagrams of the binary Lennard-Jones fluid mixtures in the pressure-temperature (a) and density temperature (b) plane for different size ratios σ_{BB}/σ_{AA} and $\Delta\mu^*$. The LJ energy parameters are the same as in Fig. 14. In (a) all liquid-vapor coexistence curves separate the vapor phase from the B-rich isotropic liquid phase. The liquid-liquid coexistence curves separate the B-rich isotropic liquid phase from the A-rich isotropic liquid phase. In (b) the full, dashed-dotted, and dotted curves enclose two-phase regions whereas the dashed lines indicate three-phase coexistence. The line code in (b) corresponds to that in (a) with the same choices of the size ratio σ_{BB}/σ_{AA} and $\Delta\mu^*$.

of thermodynamic parameters.

Figure 15 represents our numerical results for cuts through the phase diagrams of binary LJ mixtures for different size ratios σ_{BB}/σ_{AA} and chemical potential differences $\Delta\mu^*$. For the presentation we have changed the choice for $\Delta\mu^*$ along with σ_{BB}/σ_{AA} because there is no single value $\Delta\mu^*$ for which the triple points exist for the different values $\sigma_{BB}/\sigma_{AA}=1$, 1.05 , and $2^{1/3}$ (see Fig. 14). Figure 15(a) demonstrates that the liquid-vapor critical temperatures depend barely on the size ratio ($T_{c1}^{(lv)*} = 1.153$, $T_{c2}^{(lv)*} = 1.153$, and $T_{c3}^{(lv)*} = 1.152$) while the liquid-liquid critical temperatures exhibit a stronger size ratio dependence ($T_{c1}^{(ll)*} = 1.258$, $T_{c2}^{(ll)*} = 1.131$, and $T_{c3}^{(ll)*} = 1.148$). The corresponding critical densities are given by $\rho_{c1}^{(lv)*} = 0.273$, $\rho_{c2}^{(lv)*} = 0.217$, $\rho_{c3}^{(lv)*} = 0.195$ and $\rho_{c1}^{(ll)*} = 0.708$, $\rho_{c2}^{(ll)*} = 0.502$, $\rho_{c3}^{(ll)*} = 0.453$. The corresponding critical pressures of the liquid-vapor and A-rich liquid - B-rich liquid critical points are $p_{c1}^{(lv)*} = 0.113$, $p_{c2}^{(lv)*} = 0.091$, $p_{c3}^{(lv)*} = 0.083$ and $p_{c1}^{(ll)*} = 1.418$, $p_{c2}^{(ll)*} = 0.219$, $p_{c3}^{(ll)*} = 0.139$, respectively. Figure 15 shows that the A-rich liquid - B-rich liquid coexistence range within the pressure-temperature plane becomes narrower while within the density-temperature plane it grows wider with increasing size ratio.

We now turn to binary Stockmayer fluid mixtures whose components have different dipole moments and particle

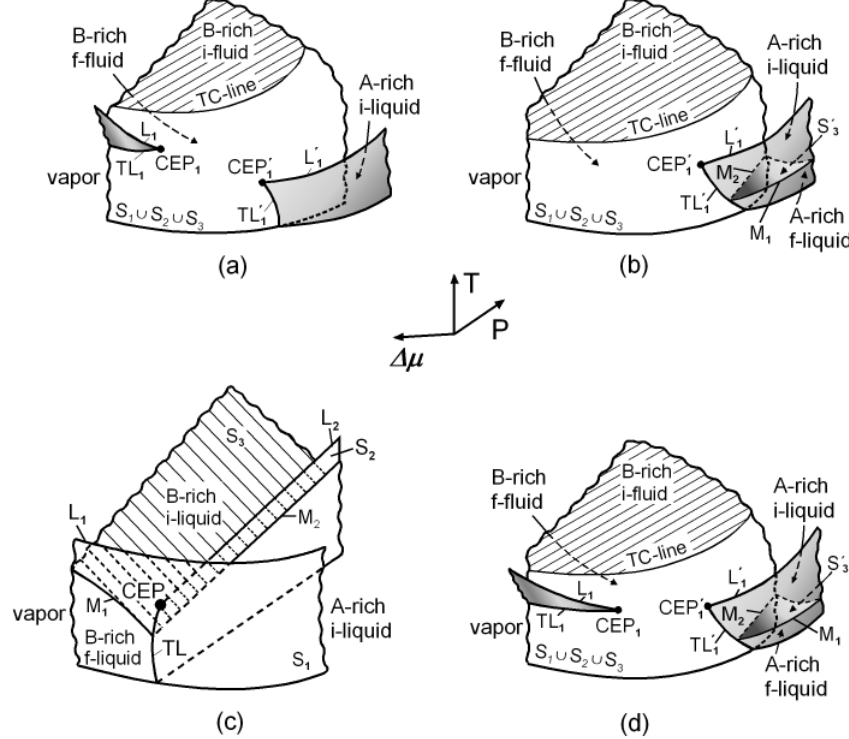


FIG. 16: Schematic bulk phase diagrams of binary Stockmayer fluid mixtures in the thermodynamic space of temperature T , pressure p , and chemical potential difference $\Delta\mu = \mu_B - \mu_A$ for various dipole moments and size parameters. The phase diagram in (a) represents a binary dipolar fluid mixture with the parameters $m_A^* = 0.75$, $m_B^* = 1.5$, and $\sigma_{BB}/\sigma_{AA} = 1$. The topology of this phase diagram is the same as that of a non-polar – dipolar binary fluid mixture with the parameters $m_A^* = 0$, $m_B^* = 1.5$, and $\sigma_{BB}/\sigma_{AA} = 1$ (compare Fig. 8(c)). Upon increasing the size of the component B such that $\sigma_{BB}/\sigma_{AA} = 2^{1/3}$ ($m_A^* = 0.75$, $m_B^* = 1.5$) one obtains the phase diagram shown in (c) in which the sheet S_3 appears again, which separates the B-rich isotropic liquid from the B-rich ferromagnetic liquid. The topology of this phase diagram is the same as that of non-polar – dipolar binary fluid mixture with the parameters $m_A^* = 0$, $m_B^* = 1$, and $\sigma_{BB}/\sigma_{AA} = 1$ (compare Fig. 8(b)). The phase diagram in (b) represents a binary dipolar fluid mixture with the parameters $m_A^* = 1$, $m_B^* = 2$, and $\sigma_{BB}/\sigma_{AA} = 1$. The topology of this phase diagram is similar to the topology of the phase diagram of non-polar – dipolar binary fluid mixture with the parameters $m_A^* = 0$, $m_B^* = 2$, and $\sigma_{BB}/\sigma_{AA} = 1$ (compare Fig. 8(c)), with the difference that at the bottom of the winglike structure attached to the surface $S_1 \cup S_2 \cup S_3$ an A-rich ferromagnetic liquid phase appears. In this phase diagram a new sheet of second-order phase transition S_3' appears, which separates the A-rich isotropic liquid from the A-rich ferromagnetic liquid. The intersection of the winglike surface and the sheet S_3' forms a line M_1 of critical end points. The intersection of the sheets $S_1 \cup S_2 \cup S_3$ and S_3' forms another line M_2 of critical end points. Upon increasing the size of the component B so that $\sigma_{BB}/\sigma_{AA} = 2^{1/3}$ ($m_A^* = 1$, $m_B^* = 2$) one obtains the phase diagram shown in (d) where a winglike surface of first-order phase transitions appears on the left part of the surface $S_1 \cup S_2 \cup S_3$. This winglike surface separates the vapor phase from the B-rich isotropic liquid phase.

sizes. This model gives a reasonable description of bidisperse ferromagnetic fluids and as such provides also a first approximation of actual polydisperse ferrocolloids. For these fluids the magnetic dipole moments of the particles are proportional to the particle volume, i.e., $m_i \propto \sigma_{ii}^3$, $i = A, B$. In the following we restrict our study to binary Stockmayer fluid mixtures with dipole moment ratio $m_B^*/m_A^* = 2$, which implies the size ratio $\sigma_{BB}/\sigma_{AA} = 2^{1/3}$. This motivates our choice of the size ratio used for the above study of the phase behavior of the binary LJ fluid mixtures.

For the dipole moment ratio $m_B^*/m_A^* = 2$ in the following we compare the phase diagrams of binary Stockmayer fluid mixtures composed of particles with either equal or different sizes. The corresponding schematic phase diagrams are shown in Fig. 16. Figure 16(a) displays the schematic phase diagrams of a binary Stockmayer fluid mixture with dipole moments $m_A^* = 0.75$, $m_B^* = 1.5$, and with particle size ratio $\sigma_{BB}/\sigma_{AA} = 1$; the LJ energy parameters are the same as in Fig. 14. The topology of this phase diagram is the same as that shown in Fig. 8(c). This fact is not surprising because in both cases $m_B^* = 1.5$ and the increase of m_A^* from $m_A^* = 0$ to $m_A^* = 0.75$ causes only a small change in the dipolar interaction energy relative to the LJ interaction energy.

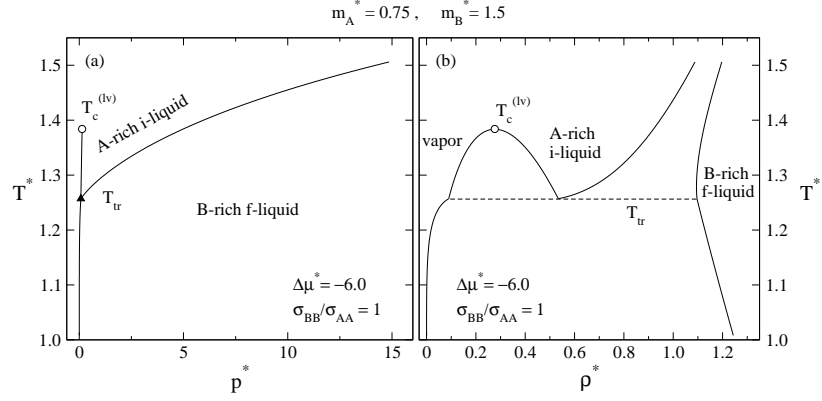


FIG. 17: Phase diagrams of a binary Stockmayer fluid mixture for dipole moments $m_A^* = 0.75$ and $m_B^* = 1.5$, and with size ratio $\sigma_{BB}/\sigma_{AA} = 1$ in the pressure-temperature (a) and density-temperature (b) plane for $\Delta\mu^* = -6$ (compare Fig. 16(a)). The LJ energy parameters are the same as in Fig. 14. Below the triple point temperature T_{tr} the isotropic vapor coexists with the B-rich ferromagnetic liquid. Between T_{tr} and $T_c^{(lv)}$ there are three phases: the vapor, the A-rich isotropic liquid, and the B-rich ferromagnetic liquid. The A-rich isotropic liquid – B-rich ferromagnetic liquid coexistence does not end in a critical point within the range of fluid densities.

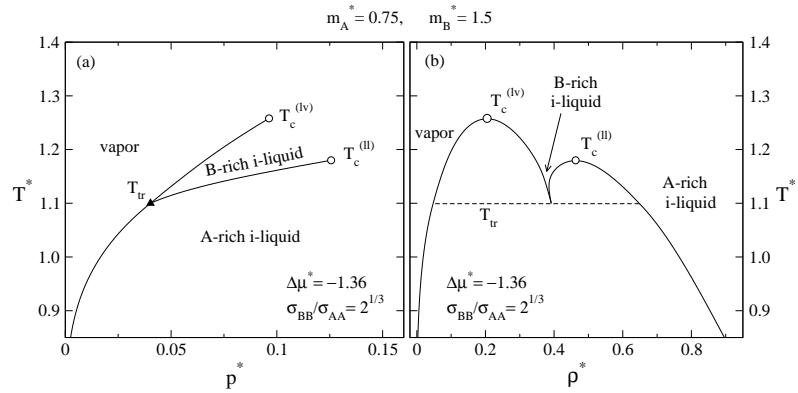


FIG. 18: Phase diagrams of a binary Stockmayer fluid mixture for dipole moments $m_A^* = 0.75$ and $m_B^* = 1.5$, and with size ratio $\sigma_{BB}/\sigma_{AA} = 2^{1/3}$ in the pressure-temperature (a) and density-temperature (b) plane for $\Delta\mu^* = -1.36$ (compare Fig. 16(c)). The LJ energy parameters are the same as in Fig. 14. Below the triple point temperature the vapor coexists with the A-rich isotropic liquid. Between T_{tr} and $T_c^{(II)}$ there are three phases: the vapor, the B-rich isotropic liquid, and the A-rich isotropic liquid. Between $T_c^{(II)}$ and $T_c^{(lv)}$ there is only vapor – B-rich isotropic liquid coexistence.

Figure 17 shows our numerical results for this binary Stockmayer fluid mixture with dipole moments $m_A^* = 0.75$ and $m_B^* = 1.5$, and with particle size ratio $\sigma_{BB}/\sigma_{AA} = 1$ for $\Delta\mu^* = -6$. Figure 17(a) demonstrates that the plane $\Delta\mu^* = -6$ cuts through the wing attached to the right hand side of the surface $S_1 \cup S_2 \cup S_3$ in Fig. 16(a). In accordance with the aforementioned topological similarity the phase diagrams shown in Fig. 17 differ from those shown in Fig. 13 only quantitatively. In Fig. 17 the liquid-vapor critical point is given by $T_c^{(lv)*} = 1.384$, $p_c^{(lv)*} = 0.138$, and $\rho_c^{(lv)*} = 0.277$. The corresponding triple point temperature and pressure are $T_{tr}^* = 1.257$ and $p_{tr}^* = 0.077$, respectively.

For the same dipole moments ($m_A^* = 0.75$ and $m_B^* = 1.5$) increasing the particle size ratio from $\sigma_{BB}/\sigma_{AA} = 1$ to $\sigma_{BB}/\sigma_{AA} = 2^{1/3}$ the phase diagram shown in Fig. 16(a) changes considerably. The resulting phase diagram is shown in Fig. 16(c). The topology of this phase diagram is the same as in Fig. 8(b). As discussed in Subsec. III B the phase diagram shown in Fig. 8(b) emerges from the phase diagram shown in Fig. 8(c) by decreasing the dipole moment m_B^* . Figure 16(a) and Fig. 16(c) show that the same topological change in the phase diagrams can be attained by increasing the corresponding particle size ratio. Figure 16(c) tells that the dipole moment strength $m_A^* = 0.75$ is

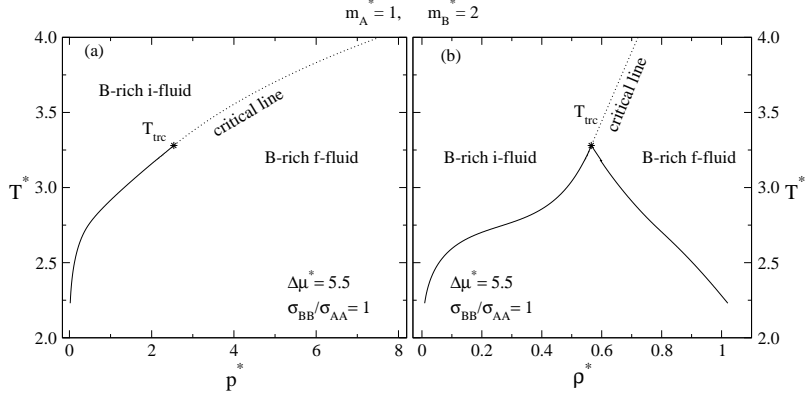


FIG. 19: Phase diagrams of a binary Stockmayer fluid mixture with dipole moments $m_A^* = 1$ and $m_B^* = 2$, and size ratio $\sigma_{BB}/\sigma_{AA} = 1$ in the pressure-temperature (a) and density-temperature (b) plane for $\Delta\mu^* = 5.5$ (compare Fig. 16(b)). The LJ energy parameters are the same as in Fig. 14. Below the tricritical temperature T_{trc} the B-rich isotropic fluid coexists with the B-rich ferromagnetic fluid. This first-order phase transition turns into a second-order phase transition at the tricritical temperature T_{trc} . Above T_{trc} the dotted line represents a line of second-order phase transitions.

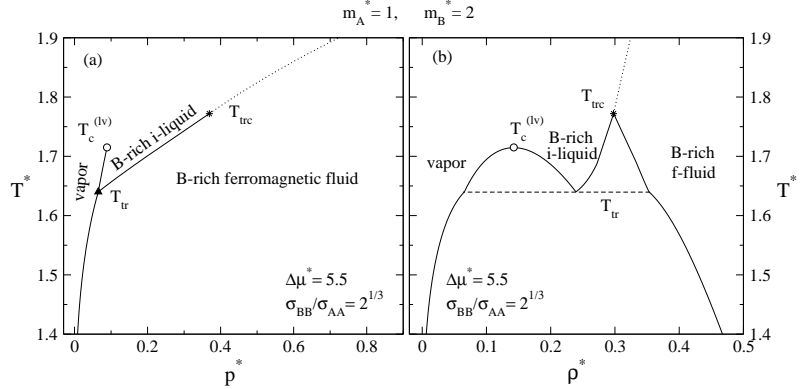


FIG. 20: Phase diagrams of binary Stockmayer fluid mixture for dipole moments $m_A^* = 1$ and $m_B^* = 2$, and with size ratio $\sigma_{BB}/\sigma_{AA} = 2^{1/3}$ in the pressure-temperature (a) and density-temperature (b) plane for $\Delta\mu^* = 5.5$ (compare Fig. 16(d)). The LJ energy parameters are the same as in Fig. 14. Below the triple point temperature T_{tr} the isotropic vapor coexists with the B-rich ferromagnetic liquid. Between T_{tr} and $T_c^{(lv)}$ there are three phases: the isotropic vapor, the B-rich isotropic liquid, and the B-rich ferromagnetic liquid. The line of first-order phase transition between the B-rich isotropic fluid and B-rich ferromagnetic liquid turns into a line of second-order phase transition (dotted line) at the tricritical temperature T_{trc} .

insufficient to lead to the formation of an A-rich ferromagnetic liquid phase, so that for negative values of $\Delta\mu^*$ the phase remains isotropic, as in the case of non-polar – polar mixtures (see Fig. 8(b)).

Figure 18 shows our numerical findings for a binary Stockmayer fluid mixture with dipole moments $m_A^* = 0.75$ and $m_B^* = 1.5$, and with particle size ratio $\sigma_{BB}/\sigma_{AA} = 2^{1/3}$ for $\Delta\mu^* = -1.36$. Figure 18(a) demonstrates that the plane $\Delta\mu^* = -1.36$ cuts through the upper part of the triple line TL in Fig. 16(c) so that the corresponding triple point T_{tr} describes a vapor – A-rich isotropic liquid – B-rich isotropic liquid coexistence with $T_{tr}^* = 1.1$ and $p_{tr}^* = 0.04$. The vapor-liquid and liquid-liquid critical points are given as $T_c^{(lv)*} = 1.258$, $p_c^{(lv)*} = 0.096$, $\rho_c^{(lv)*} = 0.204$ and $T_c^{(ll)*} = 1.18$, $p_c^{(ll)*} = 0.126$, $\rho_c^{(ll)*} = 0.462$, respectively. The topology of these phase diagrams is the same as those of shown in Fig. 2.

Increasing the dipole moments from $m_A^* = 0.75$ and $m_B^* = 1.5$ to $m_A^* = 1$ and $m_B^* = 2$ at a fixed particle size ratio $\sigma_{BB}/\sigma_{AA} = 1$ the phase diagram shown in Fig. 16(a) changes considerably leading to the phase diagram displayed in Fig. 16(b). This increase of the dipole moments causes the disappearance of the winglike structure attached to

the left part of the surface $S_1 \cup S_2 \cup S_3$ (see Fig. 16(b)), which is associated with the B-rich isotropic liquid – vapor transitions. Moreover the winglike structure attached to the right part of the surface $S_1 \cup S_2 \cup S_3$ also changes due to the appearance of the sheet S'_3 . This sheet separates the A-rich isotropic liquid at high temperatures from the A-rich ferromagnetic liquid at low temperatures. S'_3 is the locus of second-order phase transitions and is the remnant of the sheet S_3 (see Fig. 1(b)), which together with S_1 and S_2 has formed the surface $S_1 \cup S_2 \cup S_3$.

Figure 19 displays our numerical results for a binary Stockmayer fluid mixture with dipole moments $m_A^* = 1$, $m_B^* = 2$, and with particle size ratio $\sigma_{BB}/\sigma_{AA} = 1$ for $\Delta\mu^* = 5.5$. For this value of $\Delta\mu^*$ the figure shows a vertical slice through the left part of the surface $S_1 \cup S_2 \cup S_3$ in the phase diagram displayed in Fig. 16(b). The topology of these phase diagrams is the same as those of shown in Fig. 11. The tricritical point is given by $T_{trc}^* = 3.28$, $p_{trc}^* = 2.538$, and $\rho_{trc}^* = 0.565$.

Increasing the particle size ratio from $\sigma_{BB}/\sigma_{AA} = 1$ to $\sigma_{BB}/\sigma_{AA} = 2^{1/3}$ for fixed dipole moments $m_A^* = 1$ and $m_B^* = 2$, the phase diagram shown in Fig. 16(b) transforms into that shown in Fig. 16(d). Upon the increase of the particle size ratio on the left part of the surface $S_1 \cup S_2 \cup S_3$ in Fig. 16(d) a winglike structure appears, which is associated with B-rich isotropic liquid – vapor phase transitions. Through a similar topological change, the phase diagram shown in Fig. 8(d) transforms into the phase diagram shown in Fig. 8(c) upon a decrease of the dipole moment m_B^* from $m_B^* = 1.5$ to $m_B^* = 1$.

Figure 20 displays our numerical results for a binary Stockmayer fluid mixture with dipole moments $m_A^* = 1$, $m_B^* = 2$, and with a particle size ratio $\sigma_{BB}/\sigma_{AA} = 2$ for $\Delta\mu^* = 5.5$. For this choice of $\Delta\mu^*$ Fig. 20(a) represents a vertical slice through the left part of the surface $S_1 \cup S_2 \cup S_3$ in the phase diagram shown in Fig. 16(d) where the attached winglike structure appears again. The corresponding liquid-vapor critical point, the tricritical point, and the triple point are given by $T_c^* = 1.71$, $p_c^* = 0.09$, $\rho_c^* = 0.142$, $T_{trc}^* = 1.77$, $p_{trc}^* = 0.37$, $\rho_{trc}^* = 0.3$, and $T_{tr}^* = 1.64$, $p_{tr}^* = 0.065$, respectively. The topology of the phase diagrams shown in Fig. 20 is the same as of those of shown in Fig. 5.

IV. SUMMARY

In the present study of the phase behavior of binary Stockmayer (Eqs. (1)-(3)) fluid mixtures the following main results have been obtained:

(1) We have extended the one-component version of the modified mean-field density functional theory to that of binary Stockmayer fluid mixtures of particles A and B with different dipole moments, sizes, and Lennard-Jones interaction energies. In particular, we have focused on the explicit formulation of the grand canonical functional, the equilibrium pressure p , and the chemical potentials μ_A and μ_B of the two components [see Subsec. II B and Eqs. (26)-(28)].

(2) This system exhibits 6 distinct fluid phases: isotropic vapor, isotropic fluid, A-rich isotropic liquid, A-rich ferromagnetic liquid, B-rich isotropic liquid, and B-rich ferromagnetic liquid. At a given temperature T the first-order phase transitions between them follow from the equalities of the chemical potentials and of the pressure between the coexisting phases [see Subsec. II C and Eq. (35)]. The loci of the second-order phase transitions between isotropic and ferromagnetic fluids can be determined analytically from a suitable Landau theory [see Subsec. II C and Eq. (37)].

(3) In the thermodynamic parameter space $(T, p, \Delta\mu = \mu_B - \mu_A)$ we have constructed the schematic phase diagrams of binary fluid mixtures of particles with equal size and equal dipole moment (see Fig. 1). We have discussed the topological changes of these phase diagrams due to an increase of the particle dipole moments. The various shapes of the three-dimensional schematic phase diagrams are supported by numerically calculated cuts through them, which are two-dimensional phase diagrams at fixed chemical potential differences $\Delta\mu$. For dipole moments $m_A = m_B = 0$ Fig. 2 shows a cut through the phase coexistence surfaces (Fig. 1(a)) of first-order liquid-vapor and A-rich liquid – B-rich liquid phase transitions of Lennard-Jones fluid mixtures which are characterized by energy parameters ϵ_{AA} , ϵ_{BB} , ϵ_{AB} and diameters σ_{AA} , σ_{BB} , $\sigma_{AB} = (\sigma_{AA} + \sigma_{BB})/2$. For reduced dipole moments $m_A^* = m_B^* = 1$ with $m_i^* = m_i/\sqrt{\epsilon_{AA}\sigma_{AA}^3}$, $i = A, B$, Fig. 3 displays a cut through the phase coexistence surfaces (Fig. 1(b)) describing the vapor-liquid, the vapor – A-rich ferromagnetic liquid, and the A-rich isotropic liquid – B-rich isotropic liquid phase transitions of binary Stockmayer fluid mixtures. For increased dipole moments $m_A^* = m_B^* = 1.5$ the corresponding schematic phase diagram is shown in Fig. 1(c). In this case Fig. 4 shows the projections of the triple lines and critical lines onto a plane $p = \text{const}$. The vapor-liquid, vapor – ferromagnetic fluid, isotropic fluid – ferromagnetic fluid, and the A-rich ferromagnetic liquid – B-rich ferromagnetic liquid phase boundaries for dipole moments $m_A^* = m_B^* = 1.5$ are shown in Figs. 5 and 6. A further increase of the dipole moments to $m_A^* = m_B^* = 2$ leads to the schematic phase diagram shown in Fig. 1(d). A cut at $\Delta\mu^* = \text{const}$ through those coexistence surfaces is shown in Fig. 7, describing the isotropic fluid – ferromagnetic fluid and the A-rich ferromagnetic liquid – B-rich ferromagnetic liquid phase transitions.

(4) We have also constructed the schematic phase diagrams of binary fluid mixtures of non-polar and various polar particles of equal size (see Fig. 8) and have discussed the topological changes of these phase diagrams due to an increase of the dipole moment of the polar component B . For dipole moments $m_A^* = 0$ and $m_B^* = 1$ Fig. 9 shows a cut through the schematic phase diagram (Fig. 8(b)) describing the vapor-liquid, the A-rich isotropic liquid – B-rich isotropic liquid, and the vapor – ferromagnetic liquid phase coexistences. Figure 10 displays another cut at $\Delta\mu^* = \text{const}$ through the phase diagram in Fig. 8(b) indicating the possibility of A-rich isotropic liquid – B-rich ferromagnetic liquid coexistence besides the vapor-liquid one. Upon increasing the dipole moment of the polar component B from $m_B^* = 1$ to $m_B^* = 1.5$ the topology of the corresponding phase diagram shown in Fig. 8(b) changes to that shown in Fig. 8(c) which includes different types of phase coexistences: B-rich isotropic fluid – B-rich ferromagnetic fluid coexistence (see Fig. 11), A-rich isotropic fluid – B-rich ferromagnetic fluid coexistence (see Fig. 12), and vapor – A-rich isotropic liquid coexistence together with A-rich isotropic liquid – B-rich ferromagnetic liquid coexistence (see Fig. 13). A further increase of the dipole moment to $m_B^* = 2$ leads to the phase diagram shown in Fig. 8(d).

(5) We have studied the dependence of phase diagrams of binary Stockmayer liquid mixtures on the size ratio σ_{BB}/σ_{AA} . We have found that for $1 \leq \sigma_{BB}/\sigma_{AA} \leq 2^{1/3}$ the phase diagrams of binary Lennard-Jones liquid mixtures ($m_A^* = m_B^* = 0$) do not exhibit any topological change with increasing size ratio. For $m_A^* = m_B^* = 0$ Figs. 14 and 15 demonstrate that with increasing particle size ratio only the thermodynamical parameter ranges of vapor-liquid and liquid-liquid coexistence are changed. In Fig. 16 the schematic phase diagrams of binary Stockmayer liquid mixtures with particle size ratios $\sigma_{BB}/\sigma_{AA} = 1$ and $\sigma_{BB}/\sigma_{AA} = 2^{1/3}$ and for the dipole moment ratio $m_B^*/m_A^* = 2$ are shown. Such binary mixtures with dipole moment and particle size ratios different from 1 can be considered as a first approximation of polydisperse ferrofluids. The topological change of the phase diagram of binary Stockmayer liquid mixtures with dipole moments $m_A^* = 0.75$ and $m_B^* = 1.5$ due to the increase of the size ratio from $\sigma_{BB}/\sigma_{AA} = 1$ to $\sigma_{BB}/\sigma_{AA} = 2^{1/3}$ is displayed in Figs. 16(a) and 16(c). Corresponding slices through these phase diagrams for $\Delta\mu^* = \text{const}$ have been calculated (see Figs. 17 and 18). Figure 17 shows vapor – A-rich isotropic liquid and A-rich isotropic liquid – B-rich ferromagnetic liquid coexistence, while Fig. 18 displays vapor – B-rich isotropic liquid and B-rich isotropic liquid – A-rich isotropic liquid coexistence. For dipole moments $m_A^* = 1$ and $m_B^* = 2$ Figs. 16(b) and 16(d) show another type of topological change in the phase diagrams of binary Stockmayer liquid mixtures due to the increase of the size ratio from $\sigma_{BB}/\sigma_{AA} = 1$ to $\sigma_{BB}/\sigma_{AA} = 2^{1/3}$. The corresponding slices through these phase diagrams for $\Delta\mu^* = \text{const}$ have been calculated (see Figs. 19 and 20). Figure 20 shows that with increasing size ratio vapor-liquid coexistence emerges besides the coexistence of B-rich isotropic fluid and B-rich ferromagnetic fluid (Fig. 19).

[1] P. I. C. Teixeira, J. M. Tavares, and M. M. Telo da Gama, *J. Phys.: Condens. Matter* **12**, R411 (2000).

[2] B. Groh and S. Dietrich, in *New Approaches to Old and New Problems in Liquid State Theory - Inhomogeneities and Phase Separation in Simple, Complex and Quantum Fluids*, proceedings of the NATO-ASI (Series C) held in Patti Marina (Messina), Italy, July 7-17, 1998, edited by C. Caccamo, J. P. Hansen, and G. Stell (Kluwer, Dordrecht, 1999), Vol. C **529**, p. 173.

[3] T. Tlusty and S. A. Safran, *Science* **290**, 1329 (2000); S. A. Safran, *Nature Materials* **2**, 71 (2003).

[4] J. Eggebrecht, S. M. Thompson, and K. E. Gubbins, *J. Chem. Phys.* **86**, 2299 (1987).

[5] P. I. C. Teixeira and M. M. Telo da Gama, *J. Phys.: Condens. Matter* **3**, 111 (1991).

[6] P. Frodl and S. Dietrich, *Phys. Rev. E* **48**, 3741 (1993).

[7] L. X. Dang and T.-M. Chang, *J. Chem. Phys.* **119**, 9851 (2003).

[8] S. Enders, H. Kahl, M. Mecke, and J. Winkelmann, *J. Mol. Liquids* **115**, 29 (2004).

[9] A. Mukhopadhyay, C. L. Caylov, and B. M. Law, *Phys. Rev. E* **61**, R1036 (2000).

[10] A. Mukhopadhyay and B. M. Law, *Phys. Rev. E* **63**, 011507 (2000).

[11] J.-H. J. Cho and B. M. Law, *Phys. Rev. Lett.* **89**, 146101 (2002).

[12] J.-H. J. Cho and B. M. Law, *Phys. Rev. E* **67**, 031605 (2003).

[13] P. I. C. Teixeira, B. S. Almeida, M. M. Telo da Gama, J. A. Rueda, and R. G. Rubio, *J. Phys. Chem.* **96**, 8488 (1992).

[14] A. Bradbury, S. Menear, R. W. Chantrell, *J. Magn. Magn. Mater.* **54-57**, 745 (1986).

[15] K.-Y. Chan, K. E. Gubbins, D. Henderson, and L. Blum, *Mol. Phys.* **66**, 299 (1989).

[16] S. W. de Leeuw, in *Condensed Matter Theories*, edited by L. Blum and F. B. Malik (Plenum, New York, 1993), Vol. 8, p. 485.

[17] S. Jiang and K. S. Pitzer, *J. Chem. Phys.* **102**, 7632 (1995).

[18] G. T. Gao, J. B. Woller, X. C. Zeng, and W. Wang, *J. Phys.: Condens. Matter* **9**, 3349 (1997).

[19] M. J. Blair and G. N. Patey, *Phys. Rev. E* **57**, 5682 (1998).

[20] B. J. C. Cabral, *J. Chem. Phys.* **112**, 4351 (2000).

[21] T. Kristóf and I. Szalai, *Phys. Rev. E* **68**, 041109 (2003).

[22] T. Kristóf, J. Liszi, and I. Szalai, *Phys. Rev. E* **69**, 062106 (2004).

- [23] R. J. Sadus, Mol. Phys. **87**, 979 (1996).
- [24] S. W. de Leeuw, B. Smit, and C. P. Williams, J. Chem. Phys. **93**, 2704 (1990).
- [25] G. C. A. M. Mooij, S. W. de Leeuw, B. Smit, and C. P. Williams, J. Chem. Phys. **97**, 5113 (1992).
- [26] A. Müller, J. Winkelmann, T. Boublík, and J. Fischer, Mol. Phys. **78**, 121 (1993).
- [27] A. Müller, J. Winkelmann, and J. Fischer, Fluid Phase. Equilibria **99**, 35 (1994).
- [28] C. Kriebel, A. Müller, J. Winkelmann, and J. Fischer, Mol. Phys. **87**, 151 (1996).
- [29] Z. Wang and C. Holm, Phys. Rev. E **68**, 041401 (2003).
- [30] G. P. Morriss and D. J. Isbister, Mol. Phys. **59**, 911 (1986).
- [31] P. H. Lee and B. M. Ladanyi, J. Chem. Phys. **91**, 7063 (1989).
- [32] X. S. Chen, M. Kasch, and F. Forstmann, Phys. Rev. Lett. **67**, 2674 (1991).
- [33] X. S. Chen and F. Forstmann, Mol. Phys. **76**, 1203 (1992).
- [34] K. N. Trohidou and J. A. Blackman, Phys. Rev. B **51**, 11521 (1995).
- [35] A. Y. Zubarev, J. Exp. Theor. Phys. **93**, 80 (2001).
- [36] S. S. Kantorovich, J. Magn. Magn. Mater. **258-259**, 471 (2003).
- [37] S. S. Kantorovich and A. O. Ivanov, J. Magn. Magn. Mater. **252**, 244 (2002).
- [38] A. O. Ivanov and S. S. Kantorovich, Phys. Rev. E **70**, 021401 (2004).
- [39] C. Kriebel, A. Müller, J. Winkelmann, and J. Fischer, Fluid Phase Equilibria **119**, 67 (1996).
- [40] M. Wojcik and K. E. Gubbins, Mol. Phys. **51**, 951 (1984).
- [41] D. Boda, B. Kalmár, J. Liszi, and I. Szalai, J. Chem. Soc., Faraday Trans. **92**, 2709 (1996).
- [42] M. Valiskó, D. Boda, J. Liszi, and I. Szalai, Phys. Chem. Chem. Phys. **3**, 2995 (2001).
- [43] A. O. Ivanov, J. Magn. Magn. Mater. **154**, 66 (1996).
- [44] M. F. Islam, K. H. Lin, D. Lacoste, T. C. Lubensky, and A. G. Yodh, Phys. Rev. E **67**, 021402 (2003).
- [45] W. Fenz and R. Folk, Phys. Rev. E **67**, 021507 (2003).
- [46] S. Senapati and A. Chandra, J. Chem. Phys. **112**, 10467 (2000).
- [47] S. Senapati and A. Chandra, Phys. Rev. E **62**, 1017 (2000).
- [48] C. Spöler and S. H. L. Klapp, J. Chem. Phys. **118**, 3628 (2003).
- [49] M. J. Fernaud, E. Lomba, C. Martin, D. Levesque, and J.-J. Weis, J. Chem. Phys. **119**, 364 (2003).
- [50] P. Linse, J. Chem. Phys. **86**, 4177 (1987).
- [51] M. Matsumoto, Y. Takaoka, and Y. Kataoka, J. Chem. Phys. **98**, 1464 (1993).
- [52] M. Matsumoto, H. Mizukuchi, and Y. Kataoka, J. Chem. Phys. **98**, 1473 (1993).
- [53] B. Huke and M. Lücke, Rep. Prog. Phys. **67**, 1731 (2004).
- [54] S. Dietrich and A. Latz, Phys. Rev. B **40**, 9204 (1989).
- [55] S. Dietrich and M. Schick, Surf. Sci. **382**, 178 (1997).
- [56] F. Scheffler, P. Maass, J. Roth, and H. Stark, Eur. Phys. J. B **42**, 85 (2004).
- [57] I. Varga, F. Kun, and K. F. Pál, Phys. Rev. E **69**, 030501(R) (2004).
- [58] K. Mangold, J. Birk, P. Leiderer, and C. Bechinger, Phys. Chem. Chem. Phys. **6**, 1623 (2004).
- [59] G. M. Range and S. H. L. Klapp, Phys. Rev. E **69**, 041201 (2004).
- [60] G. M. Range and S. H. L. Klapp, Phys. Rev. E **70**, 031201 (2004).
- [61] G. M. Range and S. H. L. Klapp, Phys. Rev. E **70**, 061407 (2004).
- [62] J. A. Barker and D. Henderson, J. Chem. Phys. **47**, 4714 (1967).
- [63] B. Groh and S. Dietrich, Phys. Rev. Lett. **72**, 2422 (1994).
- [64] B. Groh and S. Dietrich, Phys. Rev. E **50**, 3814 (1994).
- [65] G. A. Mansoori, N. F. Carnahan, K. E. Starling, and T. W. Leland, J. Chem. Phys. **54**, 1523, (1971).
- [66] I. S. Gradshteyn and I. M. Ryzhik, in *Table of Integrals, Series, and Products*, edited by A. Jeffrey and D. Zwillinger (Academic Press, New York, 2000), p. 463.
- [67] R. L. Scott and P. H. van Konynenburg, Discuss. Faraday Soc. **49**, 87 (1970).
- [68] P. H. van Konynenburg and R. L. Scott, Philos. Trans. R. Soc. London, Ser. A **298**, 495 (1980).